

## Association between Tibetan Heat Sources and Heat Waves in China<sup>©</sup>

ZIYUAN TAN,<sup>a</sup> YUZHI LIU,<sup>a,b</sup> TIANBIN SHAO,<sup>a</sup> RUN LUO,<sup>a</sup> MIN LUO,<sup>a</sup> AND YONGKUN XIE<sup>c</sup>

<sup>a</sup> Key Laboratory for Semi-Arid Climate Change of the Ministry of Education, College of Atmospheric Sciences, Lanzhou University, Lanzhou, China

<sup>b</sup> Collaborative Innovation Center on Forecast and Evaluation of Meteorological Disasters (CIC-FEMD), Nanjing University of Information Science and Technology, Nanjing, China

<sup>c</sup> Collaborative Innovation Center for Western Ecological Safety, Lanzhou University, Lanzhou, China

(Manuscript received 27 July 2022, in final form 14 August 2023, accepted 16 August 2023)

**ABSTRACT:** The Tibetan Plateau (TP), known as the “Third Pole,” profoundly affects weather and climate at regional and global scales. In this study, we investigate the characteristics of heat waves in China and their association with the TP heat source. The results show that during the summertime from 1980 to 2020, the frequency of heat wave days that hit eastern China and northwest China increased at rates of 0.09 and 0.24 days  $\text{yr}^{-1}$ , respectively, accompanied by an increase in the atmospheric heat source (AHS) over the TP by over  $2 \text{ W m}^{-2} \text{ yr}^{-1}$  under the background of global warming. The enhanced TP heat source induces an anomalous upper-tropospheric anticyclone, which caused the western Pacific subtropical high and South Asia high to be stronger and closer to each other, causing descending motions over eastern China and consequently more heat waves. At the same time, the enhanced TP heat source weakened the westerlies, thereby favoring the occurrence and maintenance of the anticyclone centered in northwest China and creating more heat waves due to strong descending motions. Therefore, the association between the TP heat source and heat waves in China provides relevant information for studying the mechanism and future changes of heat waves.

**SIGNIFICANCE STATEMENT:** The Tibetan Plateau significantly affects the surrounding weather and climate. We find that there are some linkages between the Tibetan heat source and heat waves in China. The stronger the Tibetan heat source is, the more heat waves hit China. The enhancement of the Tibetan heat source could induce an anomalous upper-tropospheric anticyclone by affecting the western Pacific subtropical high and South Asia high, consequently causing descending motions over eastern China and the resulting heat waves. The weaker westerly due to the enhanced Tibetan heat source favors the occurrence of the anticyclone centered in northwest China, leading to more heat waves by descending motions. This study reveals a potential contributor to heat waves in China, providing some clues for better prediction in the future.

**KEYWORDS:** Asia; Atmospheric circulation; Heating; Heat wave; Summer/warm season

### 1. Introduction

Heat waves are a type of extreme weather that frequently hits all corners of the world (Lyon 2009; Cerne and Vera 2011; Cowan et al. 2014; Lu and Kueppers 2015; Rohini et al. 2016; Ward et al. 2016; Sun et al. 2018), threatening human survival, industrial and agricultural production, social and economic development, water resources, and the ecological environment (Andersen et al. 2005; Tan et al. 2007; Pechan and Eisenack 2014; Brás et al. 2021; Miller et al. 2021; Adélaïde et al. 2022). Persistent high temperatures accompanied by less rainfall can enhance drought, resulting in a reduction in the quality and yield of agricultural and forestry products (Bustan et al. 2004; Teskey et al. 2015). For example, the European heat wave in 2003 led to a significant decrease in agricultural yields and caused a decline of 30% in total primary productivity in Europe (Ciais et al. 2005).

Most importantly, heat waves have serious effects on human health and even lead to human deaths. The European heat wave in 2003 resulted in more than 70 000 deaths (Robine et al. 2008). Statistics indicate that during heat wave days, the risk of death increases by 3.74% in 43 U.S. cities (Anderson and Bell 2011). In addition, heat waves can lead to social unrest (Sanz-Barbero et al. 2018). Due to the enormous impact of heat waves on nature and human beings, they have become a hot topic in the fields of economic development, social stability, and ecological and life safety.

With global warming, considerable evidence has proven that heat waves have become stronger, longer, and more frequent over the past decades at a global scale (Meehl and Tebaldi 2004; Coumou and Rahmstorf 2012). It was found that both the intensity and extent of the heat wave that occurred in eastern Europe from July to September 2010 exceeded the heat wave occurring in Europe in 2003 (Barriopedro et al. 2011; Dole et al. 2011). Moreover, more intensive and extensive heat waves are expected to continue hitting Earth in the coming decades (Cowan et al. 2014; Lau and Nath 2014). China is one of the countries that has been strongly affected by climate change in recent decades, with significant increases in extreme

<sup>©</sup> Supplemental information related to this paper is available at the Journals Online website: <https://doi.org/10.1175/JCLI-D-22-0568.s1>.

Corresponding author: Yuzhi Liu, liuyzh@lzu.edu.cn

temperature and frequent heat waves (Ren et al. 2011; You et al. 2011; Ding et al. 2010; Luo and Lau 2017). In 2013, southern China experienced its strongest heat wave since 1951 (Zhou et al. 2014).

Observations and numerical simulations show that heat waves are influenced by many factors such as atmospheric circulation anomalies (You et al. 2011; Lau and Nath 2012; Wang et al. 2017), sea surface temperature anomalies (Hu et al. 2011), precipitation deficits (Liu et al. 2015), land surface processes (Zampieri et al. 2009), and urbanization (Lin et al. 2018). In particular, heat waves are significantly modulated by wave trains and long-term blocking high pressure in the Northern Hemisphere at middle and high latitudes (Schneidereit et al. 2012; Pfahl and Wernli 2012; Brunner et al. 2017). Meanwhile, Sutton and Hodson (2005) and Black and Sutton (2007) found that anomalies of large-scale atmospheric circulation caused by changes in sea surface temperature in the Mediterranean contributed to generating the European heat wave in 2003. Another key factor is the local land surface state, in particular the presence of dry soil moisture anomalies (Weisheimer et al. 2011). Dry soil conditions and persistent high pressure systems amplify soil moisture and temperature feedbacks and enhance surface warming (Fischer et al. 2007; Teuling et al. 2010). Moreover, the simulation results of M. Wang et al. (2013) show that urbanization has increased the average temperature of the Beijing–Tianjin–Hebei region by 0.6°C in the past 20 years, and heat waves have increased in both frequency and intensity in this region.

In addition, topography has an important impact on heat waves. Large-scale topography plays a fundamental role in setting the location of stationary climatological waves (Chang 2009; Held et al. 2002) and thus also determines the location of atmospheric blocking (Narinesingh et al. 2020), which then effects the frequency and the location of heat waves. Jiménez-Esteve and Domeisen (2022) found that the increased blocking upstream of the topography could drive an increase in heat waves. On the other hand, foehn winds generated on the leeward sides of large mountains can lead to extreme warming events (Speirs et al. 2010). Chen and Lu (2015) noted that the circulation in western North China is influenced by the downwelling topography on its western side, causing warm and dry air to sink on the leeward side, forming foehn winds and greatly increasing the temperature in the lower troposphere in the North China Plain, resulting in heat waves.

The Tibetan Plateau (TP), with an average altitude of over 4000 m, is known as the “Third Pole.” As the highest plateau in the world, the dynamic and thermal effects of the TP profoundly influence weather anomalies, climate change, material transportation such as dust, black carbon, cloud, and energy exchange in the surrounding areas (Duan et al. 2006; Yanai and Wu 2006; G. Wu et al. 2012; Xu et al. 2014; Tan et al. 2021; Zhao et al. 2023). Many researchers have studied the influence of TP thermal effects on atmospheric circulation. Reiter and Gao (1982) suggested that the heating of the TP during spring has an important role in the development and changes in the South Asia high. The uplifted TP heat source causes warming in the upper troposphere, which is closely associated with the

outbreak of the Asian summer monsoon (He et al. 1987). Zhou et al. (2009) even suggested that thermal processes over the TP may affect climate on a global scale by regulating atmosphere–ocean interactions. In recent years, significant surface and tropospheric warming have occurred over the TP, and this warming tendency is much greater than that in neighboring regions at the same latitude (Liu and Chen 2000; Niu et al. 2004; Duan et al. 2006).

Few studies have been conducted on the association of atmospheric heat source (AHS) over the TP with heat waves in eastern and northwest China. This study analyzes the variability of heat sources over the TP and the characteristics of heat waves in eastern and northwest China and discusses the mechanisms of TP heat sources that influence heat waves in these regions of China. Following the introduction of sections 1 and 2 presents the data and methods used in this study. In section 3, the distribution and tendency of heat waves in China, the TP heat source, and the mechanism by which TP heat sources influence heat waves in China are discussed. Section 4 gives a summary of the main results.

## 2. Data and methodology

### a. Datasets

Due to the lack of observational data on the TP, reanalysis data are typically used to calculate the heat source of the TP (Chan and Nigam 2009; Zhang et al. 2009; Zhu et al. 2012; Duan et al. 2014; Xie and Wang 2018; Li et al. 2019; Sun et al. 2021; Xin et al. 2022). In this study, we use the European Centre for Medium-Range Weather Forecasts (ECMWF) reanalysis, version 5, (ERA5) data (Hersbach et al. 2020) to calculate the AHS over the TP in the summer during 1980–2020. Here the summer is defined as June–August.

The temperature,  $u$  component of wind,  $v$  component of wind, vertical velocity, specific humidity, and geopotential data on pressure levels (1000–100 hPa;  $0.25^\circ \times 0.25^\circ$ ; 1980–2020; Hersbach et al. 2019a) from ERA5 are used to calculate the AHS and the atmospheric circulation indices and to analyze the mechanism of TP heat sources affecting heat waves. In addition, the 2-m temperature data on single level from ERA5 are used to investigate the characteristics of heat waves ( $0.25^\circ \times 0.25^\circ$ ; 1980–2020; Hersbach et al. 2019b).

### b. Methods

#### 1) CALCULATION OF THE TP HEAT SOURCE

Based on the atmospheric thermodynamic equations, Yanai et al. (1973) proposed a scheme for calculating the  $Q$ , which is the AHS at each pressure level:

$$Q = C_p \left[ \frac{\partial T}{\partial t} + \mathbf{V} \cdot \nabla T + \left( \frac{p}{p_0} \right)^k \omega \frac{\partial \theta}{\partial p} \right], \quad (1)$$

where  $T$  is the temperature,  $\mathbf{V}$  is the horizontal wind vector,  $\omega$  is the vertical velocity,  $p$  denotes the pressure, the surface pressure  $p_0 = 1000$  hPa,  $\theta$  is the potential temperature,  $k = R/C_p$ ,  $C_p = 1004.64 \text{ J (K kg)}^{-1}$ , and  $R = 287 \text{ J (K kg)}^{-1}$ . Assuming that

$\omega = 0$  at the top of the troposphere, integrating Eq. (1) over the whole atmosphere, Eq. (2) is obtained:

$$\int_{p_t}^{p_s} Q dp = \frac{C_p}{g} \int_{p_t}^{p_s} \frac{\partial T}{\partial t} dp + \frac{C_p}{g} \int_{p_t}^{p_s} \mathbf{V} \cdot \nabla T dp + \frac{C_p}{g} \int_{p_t}^{p_s} \left( \frac{p}{p_0} \right)^k \omega \frac{\partial \theta}{\partial p} dp, \quad (2)$$

where  $p_s = 1000$  hPa and  $p_t = 100$  hPa. The term on the left side of Eq. (2) ( $\int_{p_t}^{p_s} Q dp$ ) is the calculation of the whole layer AHS adopted in this study. The three terms on the right side from left to right in Eq. (2) denote the local time derivative of temperature, temperature advection, and vertical diabatic heating, respectively.

## 2) DEFINITION OF HEAT WAVES

There are many definitions of heat waves (Smith et al. 2013; You et al. 2017) based on different temperature data (daily maximum, daily minimum, daily average), different durations (one or several days) and different temperature thresholds. According to different temperature thresholds, a heat wave can be defined in two ways. In the first heat wave definition, a fixed temperature threshold is used. For example, the World Meteorological Organization suggests that the criterion for heat waves is a maximum daily temperature above 32°C lasting for more than 3 days (Smoyer-Tomic et al. 2003). In the second definition, a percentage of a regional climatology factor is used as the high temperature threshold, such as the 95th percentile based on the daily mean temperature (Anderson and Bell 2011).

This study adopts the first heat wave definition, with the daily maximum temperature equal to or greater than 35°C for more than 3 consecutive days as the definition (Tan et al. 2007), which is given by the China Meteorological Administration according to the geographical location and climate of China. This definition has a uniform standard for heat waves in each region, the threshold of 35°C can better reflect the characteristics of high temperatures during heat waves and is more consistent with general perception and body feeling.

## 3) DEFINITIONS OF THE WPSH INDEX, SAH INDEX, AND WESTERLY INTENSITY

Western Pacific subtropical high (WPSH) index: On the 500-hPa isobaric surface, within 110°E–180° and north of 10°N, the area of the grid with geopotential greater than 5880 gpm is defined as the WPSH area index:

$$\text{Area index}_{\text{WPSH}} = \sum \sum (n_{ij} \times \cos \phi_j) d_x d_y, \quad (3)$$

where  $i$  is the latitudinal serial number of the grid point,  $j$  is the longitudinal serial number of the grid point,  $\phi$  is the latitude at the  $j$ th grid point,  $d_x$  is the latitudinal grid point distance, and  $d_y$  is the longitudinal grid point distance. If the geopotential is greater than 5880 gpm,  $n_{ij} = 1$ , otherwise the  $n_{ij} = 0$ .

The sum of the difference between the geopotential of all grid points with geopotential greater than 5880 and 5880 gpm is defined as the WPSH intensity index; and the longitude of the westernmost position of the 5880-gpm contour in the range of 90°E–180° is defined as the west extending point.

South Asian high (SAH) index: On the 200-hPa isobaric surface, at 10°–50°N, 110°E–180°E, the area of the grid with geopotential greater than 12500 gpm is defined as the SAH area index:

$$\text{Area index}_{\text{SAH}} = \sum \sum (n_{ij} \times \cos \phi_j) d_x d_y, \quad (4)$$

where  $i$  is the latitudinal serial number of the grid point,  $j$  is the longitudinal serial number of the grid point;  $\phi$  is the latitude at the  $j$ th grid point,  $d_x$  is the latitudinal grid point distance and  $d_y$  is the longitudinal grid point distance. If the geopotential is greater than 12500 gpm,  $n_{ij} = 1$ ; otherwise,  $n_{ij} = 0$ .

The sum of the difference between the geopotential of all grid points with geopotential greater than 12500 and 12500 gpm is defined as the SAH intensity index; and the longitude of the easternmost position of the 12500-gpm contour in the range of 90°E–180° is defined as the east extending point.

In addition, the average  $u$ -component wind in the range of 30°–50°N, 80°–120°E at 200 hPa is defined as the westerly intensity.

Due to the relatively narrow latitude ranges in this study, we do not consider the actual area represented by a grid point but weight them equally when computing the AHS, intensity indices of WPSH, SAH, and the intensity of the westerlies.

## 3. Distribution and tendency of heat waves in China

Figures 1a and 1b show the spatial distribution and tendency of the number of heat wave days in China during the summer of 1980–2020. As indicated in Fig. 1a, heat waves in China during the past 41 years have mainly occurred in northwest China, eastern China, and the Sichuan Basin. Simultaneously, obvious tendencies of heat wave days in the period 1980–2020 are found in the above regions (Fig. 1b). In this study, considering the region size, we mainly analyze the heat wave features in northwest China and eastern China. As shown in Fig. 1c, the northern side of the TP and west of the Yellow River is defined as northwest China (enclosed by the red curve in Figs. 1a,b). The area in the east side of the altitude of 500 m from the North China Plain to southern China is defined as eastern China (enclosed by the blue curve in Figs. 1a,b).

Within China, northwest China has the highest number of heat wave days, mostly in the Tarim Basin, Junggar Basin, Turpan Basin, and western Inner Mongolia. These four regions, except the Turpan Basin, are distributed within the Taklamakan Desert, Gurbantunggut Desert, and Gobi Desert. The special land types such as desert and gobi and the desert climate in these areas are important reasons for the frequent occurrence of heat waves. On average, annual heat wave occurs in the eastern Tarim Basin and Turpan Basin for more than 40 days  $\text{yr}^{-1}$ , with a maximum of 74.0 days  $\text{yr}^{-1}$ , meaning that, in a few areas, more than two-thirds of summer days

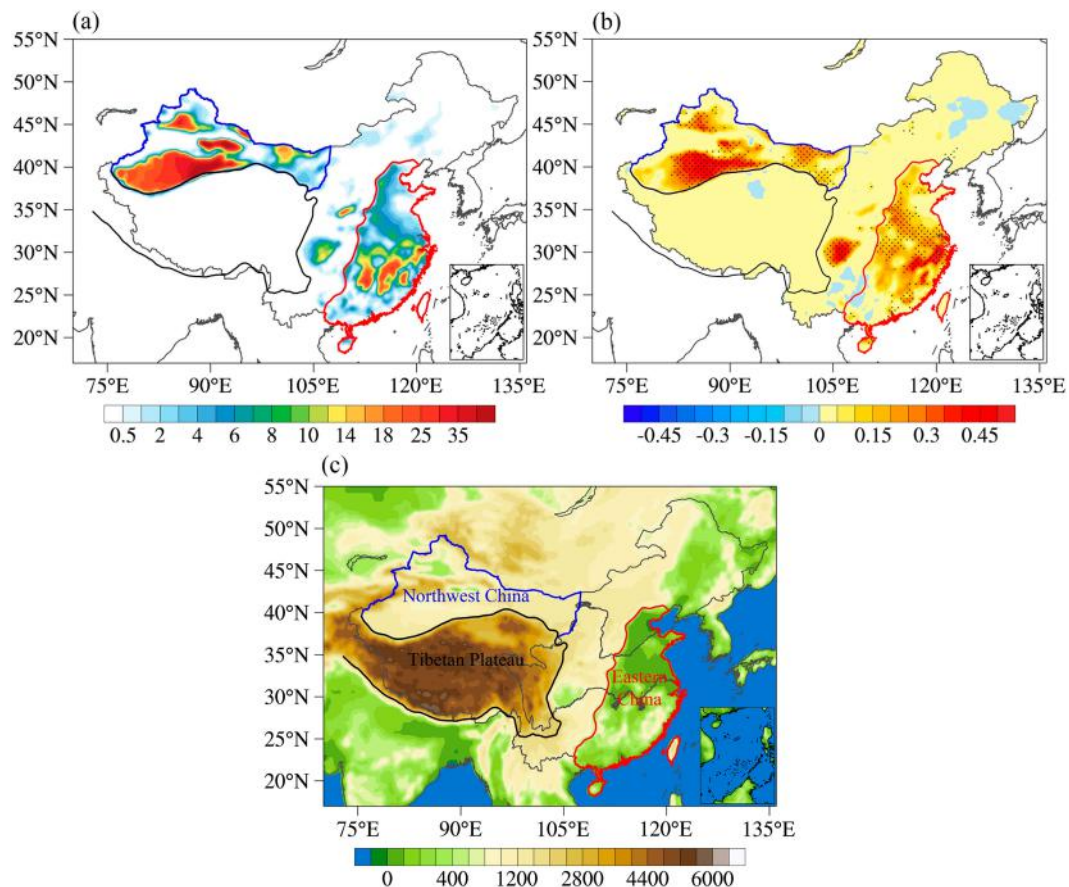


FIG. 1. Spatial distribution of long-term (a) means (unit: days) and (b) trends (unit: days yr<sup>-1</sup>) of the number of heat wave days in summer during 1980–2020. The black dotted area in (b) indicates the trends are significant at the 90% confidence level. (c) Topography and regional divisions of the study area. The red and blue curves denote the zones of eastern China and northwest China, respectively. The black curve is the contour at an altitude of 2000 m, which indicates the TP.

have a daily maximum temperature of 35°C or higher. The average annual number of heat wave days for the whole of northwest China was 10.2 days yr<sup>-1</sup> during the past 41 years. The number of heat waves in eastern China is less than those in northwest China, with most heat waves occurring in the middle and lower reaches of the Yangtze River and along the Taihang Mountains from northern eastern China to the Huai River. The heat wave days in the middle and lower reaches of the Yangtze River are 20–25 days yr<sup>-1</sup>, with a maximum of 31.2 days yr<sup>-1</sup>. In the past 41 years, there have been 5.2 days of annual mean heat wave days in eastern China.

There is a significant increase in heat waves in northwest and eastern China (Fig. 1b). The average tendency of heat wave days in northwest China is 0.24 days yr<sup>-1</sup>; the area with the largest increase is located in the eastern Tarim Basin with a maximum value of 0.55 days yr<sup>-1</sup>. On average, the increase in heat wave days in eastern China is 0.09 days yr<sup>-1</sup>; the areas with the strongest increases are located mainly in the North China Plain, which has an increase of 0.15–0.25 days yr<sup>-1</sup>. These increases are significantly larger in the middle and lower reaches of the Yangtze River, where they are above

0.35 days yr<sup>-1</sup>. Northwest and eastern China are facing severe challenges of heat wave hitting.

Overall, it can be found that most of the heat wave events occur after 2000 in eastern and northwest China, while the heat wave low-occurrence years are concentrated before 2000. It also indicates that the number of heat wave days is overall higher in the recent 20 years after 2000 than for the years before 2000 (Fig. S1a in the online supplemental material). The high-occurrence years of heat waves in northwest China are mainly concentrated in three periods, 1994–2002, 2006–11, and 2015–17, whereas the heat waves in eastern China show a fluctuating increase with three obvious peaks occurring in 1988, 2003, and 2013. On the whole, heat wave days in eastern China are a third to a half of those in northwest China.

#### 4. Association between China's heat wave and TP heat source

The thermal effect of the TP in summer has an important impact on the surrounding weather and climate. Figure 2 shows the spatial distribution and tendency of the AHS over the TP

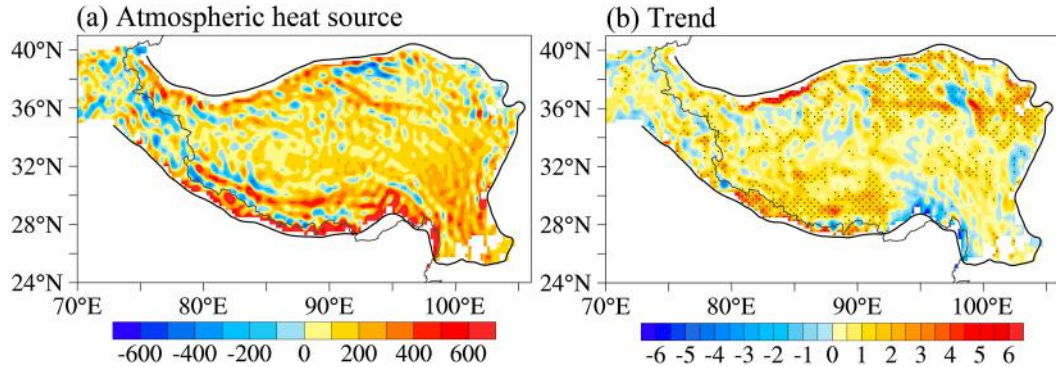


FIG. 2. Spatial distributions of long-term (a) means (unit:  $\text{W m}^{-2}$ ) and (b) trends (unit:  $\text{W m}^{-2} \text{ yr}^{-1}$ ) of the AHS over the TP in summer during 1980–2020. The black dotted areas indicate the trends are significant at the 90% confidence level. The black curve is the contour at an altitude of 2000 m, which indicates the TP.

from 1980 to 2020. As shown in Fig. 2a, most of the TP acts as a heat source in summer, with an average of  $116.6 \text{ W m}^{-2}$ . The AHS is stronger over the eastern and southern TP than over the western and northern TP. The AHS values over the southeastern TP range from  $200$  to  $400 \text{ W m}^{-2}$ . The AHS over most areas of the TP tends to be significantly enhanced, with an average increase of  $0.66 \text{ W m}^{-2} \text{ yr}^{-1}$  (Fig. 2b). The enhancements are more obvious in the northeast, southwest, and east of the TP, which are more than  $2.5$ ,  $2$ , and  $1.5 \text{ W m}^{-2}$ , respectively. According to the time series of the regional average AHS and its three components (Fig. S2), the AHS and vertical diabatic heating indicate increasing trends, while the temperature advection shows decreasing trends. In terms of magnitude and tendency, vertical diabatic heating accounts for the largest contribution to the AHS over the TP.

From Fig. 3a, the AHS over the TP is positively correlated with the number of heat wave days in China. The areas where heat waves are significantly correlated with the AHS on the TP are mainly distributed in the heat wave high-occurrence areas in northwest China and the middle and lower reaches of the Yangtze River and southern eastern China. The correlations between the AHS over the TP and heat waves are stronger in northwest China than in eastern China (Fig. 3a). The significant correlation coefficients between the AHS and heat waves over the TP in northwest China are mostly in the range of  $0.3$ – $0.4$ , and some regions can reach  $0.5$  or more. We also give the results of correlation coefficients after detrending. As shown in Fig. 3b, although the correlation between the AHS over the TP and heat waves in China weakens after detrending, which implies that the linear trend plays a major role in the significantly positive correlation between AHS over the

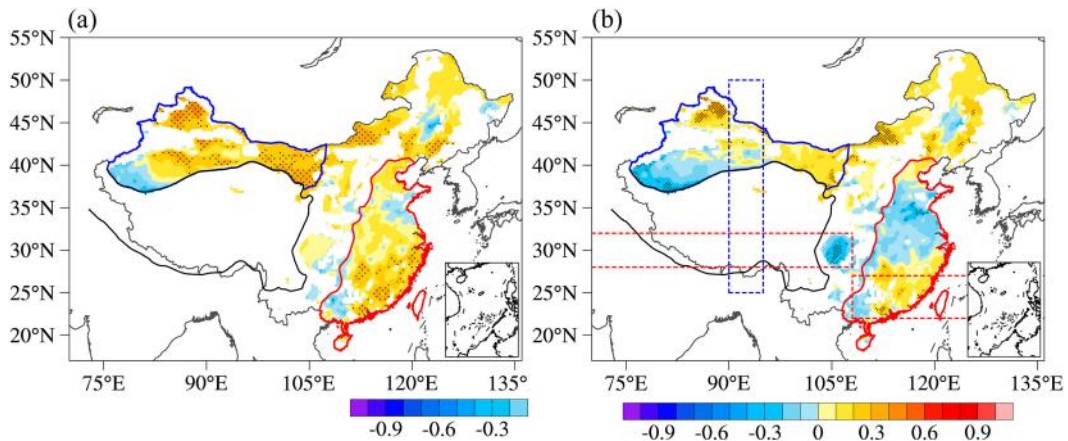


FIG. 3. Spatial distribution of (a) correlation coefficients between regional average AHS over the TP and heat wave days and (b) correlation coefficients between detrended regional average AHS over the TP and detrended heat wave days in summer during 1980–2020. The black dotted areas indicate the correlations are significant at the 90% confidence level. The red and blue curves denote the zones of eastern China and northwest China, respectively. The black curve is the contour at an altitude of 2000 m, which indicates the TP. The red dashed boxes (TP:  $28^\circ$ – $32^\circ\text{N}$ ; eastern China:  $22^\circ$ – $27^\circ\text{N}$ ) and blue dashed boxes ( $90^\circ$ – $95^\circ\text{E}$ ) in (b) indicate the locations of the cross sections of meteorological element anomalies for the heat wave anomalous years in eastern China and northwest China in the later text, respectively.

TP and the heat wave days in China, it can be found that the regions with significant positive correlation without detrending (such as southeastern China and eastern and northern northwest China) still maintain positive correlation after detrending. In summary, the positive correlation of the AHS over the TP with heat waves in northwest China and eastern China suggests that the TP thermal effect in summer could possibly contribute to the occurrence of heat waves in the surrounding areas.

To investigate the effect of the TP heat sources on heat waves in eastern China and northwest China, the 11 years with higher and lower heat wave days in the two regions are selected based on the first quartile and third quartile of the regional average of heat wave days in eastern China and northwest China in summer 1980–2020 after detrending (Fig. S1b), respectively, which are listed in Table 1.

Figure 4 shows the anomalies of AHS over the TP in heat wave anomalous years, which are the average AHS over the TP in the heat wave high-occurrence years of eastern China minus the average AHS over the TP in the heat wave low-occurrence years of eastern China. For the heat wave anomalous years of eastern China (Fig. 4a), the positive anomalies of AHS over the TP are mainly distributed in the southwestern and northeastern areas of the TP, with anomalies above  $40 \text{ W m}^{-2}$ , and the anomalies are stronger in the southwestern TP. Meanwhile, the spatial distributions of the AHS anomalies over the TP are similar to the tendencies of the AHS in Fig. 2b. It is suggested that the strengthening of the AHS in these regions may cause the positive AHS anomalies over the TP in heat wave anomalous years of eastern China. The distribution of the AHS anomalies over the TP in the heat wave anomalous years of northwest China is also dominated by positive anomalies over the southwestern and northeastern TP (Fig. 4b). These positive anomalies of AHS are stronger than those in the heat wave anomalous years of eastern China, especially over the southwestern TP, where the positive anomalies are more than  $90 \text{ W m}^{-2}$  (Fig. 4b). Besides, the regional average AHS anomalies over the TP in the heat wave anomalous years of eastern China ( $2.96 \text{ W m}^{-2}$ ) are lower than those of northwest China ( $7.10 \text{ W m}^{-2}$ ). Although the spatial distributions of the TP heat source anomalies during the years with heat wave anomalies in eastern and northwest China are similar, there are still some differences due to the different heat wave high-occurrence and the low-occurrence years of eastern and northwest China.

## 5. Mechanism of TP heat source influencing heat waves in China

### a. The effect of TP heat source on the formation of heat waves in eastern China

The anomaly of the TP heat source may cause changes in the atmospheric circulation and weather systems in the surrounding and downstream areas. From Fig. S3a, the area and intensity of the WPSH have expanded and intensified, accompanied by westward extension during the past 41 years with the increase in the AHS over the TP. The AHS over the TP is positively correlated with the area index and intensity index of the WPSH, which are negatively correlated with the west extending point of

TABLE 1. Heat wave high-occurrence years and low-occurrence years of eastern China and northwest China in summer during 1980–2020 after detrending.

High-occurrence year		Low-occurrence year	
Eastern China	Northwest China	Eastern China	Northwest China
1981	1997	1982	1981
1983	1999	1986	1989
1988	2000	1987	1992
1990	2001	1993	1993
1992	2002	1996	2003
1998	2006	1997	2005
2003	2008	1999	2012
2005	2010	2008	2013
2010	2011	2014	2014
2013	2015	2015	2019
2017	2016	2020	2020

the WPSH, indicating that the stronger the TP heat source in summer is, the stronger the intensity and larger the range of the WPSH. The area and intensity of the SAH also show expanding and strengthening tendencies (Fig. S3b), as well as the eastward extension of the eastern extension point. The AHS over the TP is positively correlated with the area index, intensity index, and east extending point of the SAH, indicating that the stronger the TP heat source is in summer, the stronger the SAH. After detrending (Table 2), although the correlations of the detrended AHS over the TP with the detrended WPSH index and SAH index become weaker, it still shows that the stronger the AHS over TP, the larger the area and the stronger the intensity of the WPSH and SAH. Some studies also show that the strengthening of TP heat source has an important effect on the WPSH and SAH. (Shi et al. 2019; Liu et al. 2020; Ge et al. 2019). Zhong et al. (2008) showed that in years with stronger (weaker) summer heat sources over the TP, the WPSH strengthened (weakened) and extended westward (retreated eastward); the SAH also strengthened (weakened) and expanded eastward (extended westward). The above analysis indicates that the increase in the AHS over the TP has close relationships with the SAH around the TP and WPSH downstream of the TP.

Furthermore, Table S1 gives the correlations of the three components of the AHS over the TP with the WPSH and SAH indices. The area index and intensity index of the WPSH and SAH are negatively correlated with temperature advection and positively correlated with vertical diabatic heating with the largest correlation. After detrending (Table 2), the correlations of the detrended AHS components over the TP with the detrended WPSH index and SAH index weaken and are insignificant but still indicate to some extent that the detrended area index and intensity index of the WPSH and SAH are negatively correlated with the detrended temperature advection and positively correlated with the detrended vertical diabatic heating. The correlations of the detrended AHS components over the TP with the detrended WPSH index and SAH index are relatively weaker, which, due to the linear trend, play a major role. Meanwhile, some previous studies also indicate that the stronger the

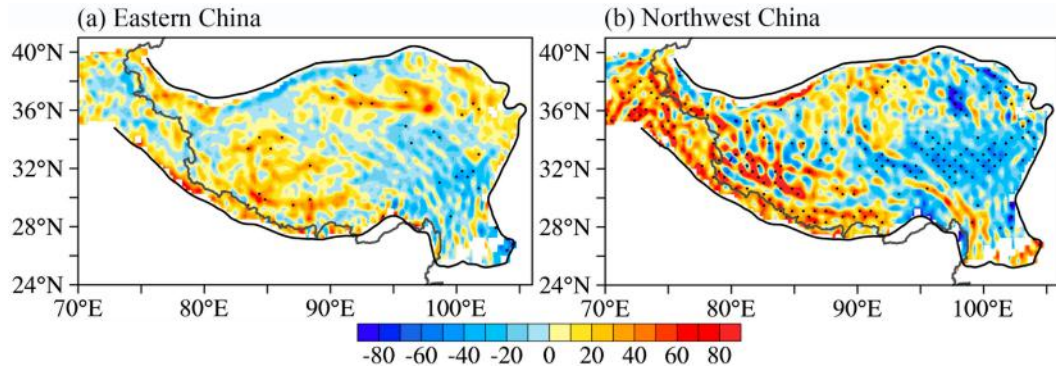


FIG. 4. Anomalies of the AHS (unit:  $\text{W m}^{-2}$ ) over the TP between the heat wave high-occurrence years and low-occurrence years of (a) eastern China and (b) northwest China in summer during 1980–2020 after detrending. The black dotted areas indicate the anomalies are significant at the 90% confidence level. The black curves are the contours at an altitude of 2000 m, which indicates the TP.

vertical diabatic heating over the TP in summer is, the stronger the WPSH and SAH. Zhu et al. (2023) found that the stronger summer vertical diabatic heating over the TP is conducive to the enhancement and mutual proximity of the SAH and the WPSH by vertical motions over the TP and the western Pacific. Lu et al. (2023) also concluded that the enhanced diabatic heating over the southern TP makes the SAH intensify and extend eastward, accompanied by the WPSH intensifying and extending westward.

Figure S4 shows the distribution of the correlation coefficients of the WPSH indices and the SAH indices with the number of heat wave days in summer from 1980 to 2020. It shows that the WASH and SAH are significantly related to the heat waves in eastern China. The area index and intensity index of the WPSH are positively correlated with heat wave days during summer in eastern China (Figs. S4a–c). The west extending point of the WPSH is significantly negatively correlated with heat wave days in eastern China. On the other hand, the area index, intensity index, and east extending point of the SAH are significantly positively correlated with the number of heat wave days in eastern China in summer. After detrending, the correlations of the detrended WPSH index and SAH index with the detrended number of heat wave days weakens (Fig. 5), while the correlations of the detrended WPSH index and SAH index with the detrended number of heat wave days are similar with those without detrending. The correlations of the detrended area index and intensity index of the WPSH with detrended heat wave days

during summer in eastern China can reach 0.2, especially in the middle and lower reaches of the Yangtze River (Figs. 5a,b). The correlation coefficients of the detrended west extending point of the WPSH with detrended heat wave days in eastern China are less than  $-0.3$ . The correlation coefficients of the detrended area index, intensity index, and east extending point of the SAH with the detrended number of heat wave days in eastern China in summer range from 0.1 to 0.4.

The average 5880-gpm geopotential height contour at 500 hPa and 12 500-gpm geopotential height contours at 200 hPa in the heat wave anomalous years of eastern China are used to represent the distribution of the WPSH and SAH in these years of eastern China, respectively (Fig. 6). The WPSH extends west to  $128^{\circ}\text{E}$  and the SAH extends east to  $127.5^{\circ}\text{E}$  in heat wave high-occurrence years of eastern China, whereas the WPSH shrinks eastward to  $129.5^{\circ}\text{E}$  and the SAH shrinks westward to  $125^{\circ}\text{E}$  in heat wave low-occurrence years. This means that the larger and stronger the WPSH and SAH are and the closer they are to each other, the more heat waves occur in eastern China in summer. Consistent with the correlations of the AHS over the TP with the west extending point of the WPSH and the east extending point of the SAH (Table 2 and Table S1), when the TP heat source is strong, the WPSH is more westward and the SAH is more eastward, indicating that the TP heat source influences the occurrence of heat waves in eastern China in summer by affecting the WPSH and SAH.

TABLE 2. Correlations of the detrended AHS and components over the TP with the detrended WPSH index, SAH index and westerly intensity in summer during 1980–2020.

	WPSH			SAH		
	Area index	Intensity index	West extending point	Area index	Intensity index	East extending point
AHS	0.129	0.151	$-0.146$	0.118	0.169	$-0.038$
Local time derivative of temperature	0.142	0.208	$-0.151$	0.128	0.170	0.066
Vertical diabatic heating	0.118	0.135	$-0.128$	0.105	0.150	$-0.047$
Temperature advection	$-0.099$	$-0.118$	0.039	$-0.049$	$-0.054$	0.075

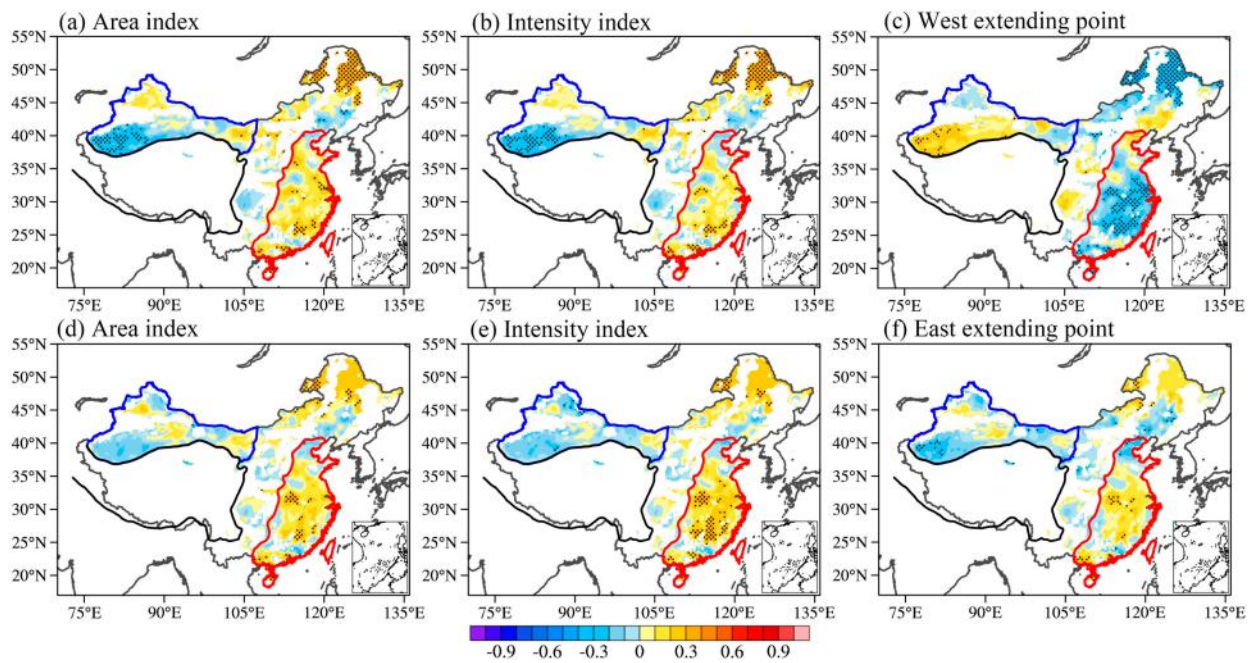


FIG. 5. Correlations of the detrended (a)–(c) WPSH index and (d)–(f) SAH index with the detrended number of heat wave days in summer during 1980–2020. The black dotted areas indicate the correlations are significant at the 90% confidence level. The red and blue curves denote the zones of eastern China and northwest China, respectively. The black curve is the contour at an altitude of 2000 m, which indicates the main body of the TP.

To investigate the mechanism of the TP heat source that influences summer heat waves in eastern China, the distribution of geopotential height fields at different layers and the latitudinal cross section of mean geopotential height anomalies at

28°–40°N in the heat wave anomalous years of eastern China are shown in Fig. 7. In the heat wave high-occurrence years of eastern China, the center of the SAH is located over the southern edge of the TP and extends eastward to the west Pacific, affecting all of eastern China (Fig. 7a). The WPSH expands westward to 128°E at 500 hPa (Fig. 7b). Generally, the lower troposphere near the WPSH ridge axis is in descending motion, with a small pressure gradient and weak wind speed, which is favorable for the occurrence of heat waves. Meanwhile, eastern China is influenced by the WPSH at 850 hPa (Fig. 7c). From the geopotential height anomalies (Figs. 7d–f), there are strong anomalous anticyclones in the upper troposphere on the east side of the TP, and the anomalous anticyclones extend southeast from northern eastern China at 500 hPa to all of eastern China at 850 hPa. This anomalous anticyclone migrated eastward from the upper layers to the lower layers, which strengthened the westward extension of the WPSH, resulting in the WPSH and SAH being closer to each other.

The anomalies of geopotential height caused by the TP heat source are a “cyclone–anticyclone–cyclone” distribution in mid-latitudes region, showing a zonal wave train pattern over the Eurasian continent, which is more obvious in the middle and low levels (Figs. 7d–f). This wave train pattern is also evident from the cross section of the geopotential height anomalies (Fig. 7g). The wave train-like pattern is related to the circumglobal teleconnection revealed in previous studies (Ding and Wang 2005). A significant correlation between heat waves in southeastern China and the circumglobal teleconnection has been noted on interannual time scales (W. Wang et al. 2013). The anomalous TP

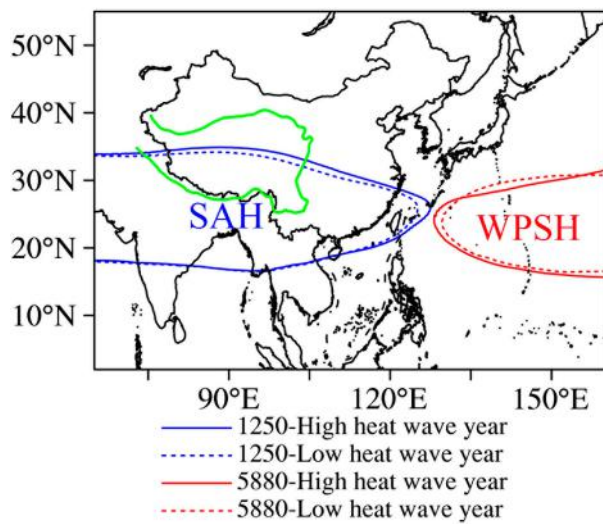


FIG. 6. Distribution of the SAH at 200 hPa (1250-gpm contour of geopotential height) and the WPSH at 500 hPa (5880-gpm contour of geopotential height) for the summer of heat wave high-occurrence years and low-occurrence years of eastern China during 1980–2020 after detrending. The green curve is the contour at an altitude of 2000 m, which indicates the TP.

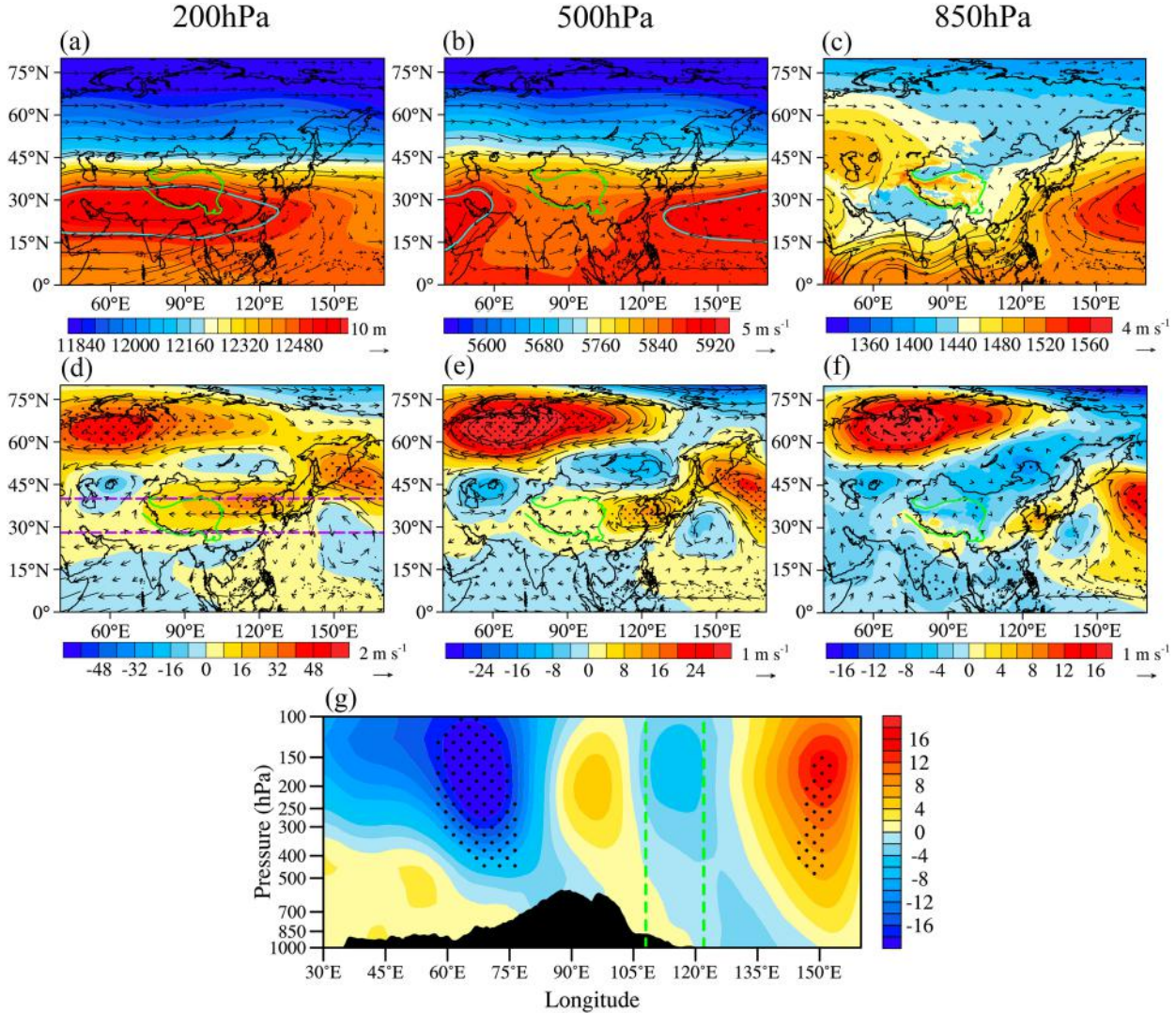


FIG. 7. Mean summer geopotential height fields (color; unit: gpm) and horizontal wind fields (vectors; unit:  $\text{m s}^{-1}$ ) of (a) 200, (b) 500, and (c) 850 hPa in the summer of the heat wave high-occurrence years of eastern China and (d)–(f) the anomalies of geopotential height (color; unit: gpm) and horizontal wind fields (vectors; unit:  $\text{m s}^{-1}$ ) between the heat wave high-occurrence years and low-occurrence years in summer during 1980–2020 after detrending. The blue curves in (a) and (b) are the contours at 12500 and 5880 gpm, respectively. The green curves are the contours at an altitude of 2000 m, which represent the TP. The purple dashed lines in (d) indicate the location of the cross section of the anomalies of the mean geopotential height field in (g). (g) The cross section of the anomalies of the mean geopotential height field at 28°–40°N between the heat wave high-occurrence years and low-occurrence year. The black shading indicates topography. The dashed green lines indicate the location of eastern China. The black dotted areas in (d)–(g) indicate the anomalies are significant at the 90% confidence level.

heating can modify the atmospheric circulation by initiating Rossby waves propagating eastward (Wang et al. 2008), thus affecting the heat waves in eastern China.

The latitudinal wave train pattern caused by the TP heat source makes WPSH and SAH close to each other, so we check the latitudinal cross section in the vertical direction of the geopotential height anomalies. From the mean cross section of the geopotential height anomalies (Fig. 7g), an anomalous high pressure exists over the TP and tilts slightly eastward from the middle layers to the lower layers, affecting the weather in eastern China. Meanwhile, anomalous high

pressure also exists over the west Pacific Ocean east of 130°E, indicating that the WPSH is anomalously strong in heat wave high-occurrence years of eastern China.

According to the spatial distribution of the anomalies of AHS over the TP (Fig. 4a) and the correlation coefficients between detrended regional average AHS over the TP and detrended heat wave days (Fig. 3b), we select the location of the cross section of the temperature, vertical velocity, wind field, specific humidity, and their anomalies (see Fig. 3b). From the latitudinal cross section of the mean vertical velocity, wind field, temperature, specific humidity, and their anomalies at

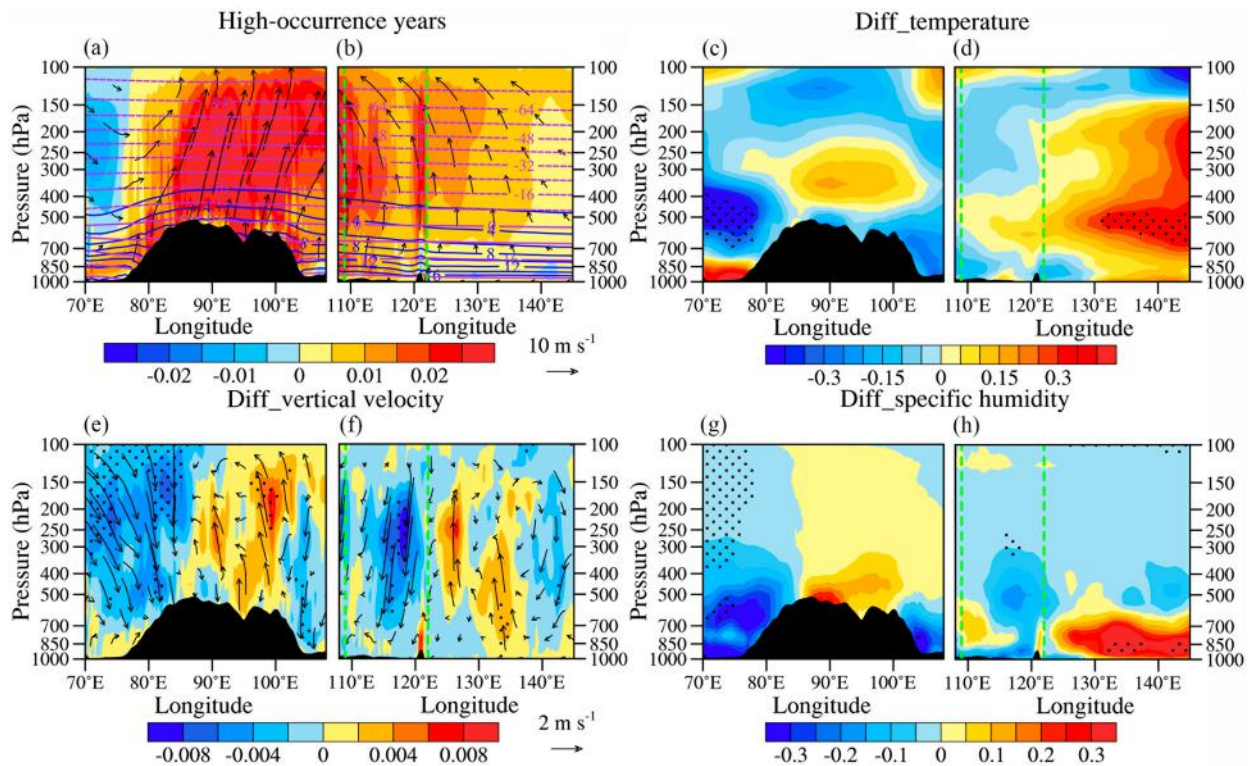


FIG. 8. (a),(b) Cross section of the mean temperature (purple contours, unit:  $^{\circ}\text{C}$ ), vertical velocity (color; unit:  $\text{m s}^{-1}$ , positive values indicate ascending motion), wind field (vectors of  $u$  and  $w \times 1500$ ; unit:  $\text{m s}^{-1}$ ) and specific humidity (blue contours; unit:  $\text{g kg}^{-1}$ ) over the TP ( $28^{\circ}$ – $32^{\circ}\text{N}$ ) and eastern China ( $22^{\circ}$ – $27^{\circ}\text{N}$ ) in the summer of the heat wave high-occurrence years of eastern China and (c)–(h) the anomalies between the heat wave high-occurrence years and low-occurrence years over (c),(e),(g) the TP and (d),(f),(h) eastern China. The black shading indicates topography. The dashed green lines indicate the location of eastern China. The black dotted areas in (b)–(h) indicate the anomalies are significant at the 90% confidence level.

$28^{\circ}$ – $32^{\circ}\text{N}$ , strong ascending motions exist from the lower layers to upper layers over the TP (Fig. 8a) and over the Pacific Ocean east of  $122^{\circ}\text{E}$  (Fig. 8b) in the heat wave high-occurrence years of eastern China. During these years, there are positive temperature anomalies from the lower layers to  $250 \text{ hPa}$  over the TP (Fig. 8c), corresponding to the region with positive heat source anomalies. In the western Pacific east of  $122^{\circ}\text{E}$ , there are also strong positive temperature anomalies from the lower layers to upper layers (Fig. 8b). In eastern China, there are positive temperature anomalies over  $400$ – $700 \text{ hPa}$  and near the surface, indicating strong heat waves (Fig. 8d). Combined with the anomalous geopotential in Fig. 7g, this indicates that both the SAH and the WPSH are anomalously strong in the heat wave high-occurrence years of eastern China.

As for the vertical velocity anomalies and wind field anomalies, positive vertical velocity anomalies over the TP (Fig. 8e), especially at  $86^{\circ}$ – $102^{\circ}\text{E}$ , also correspond to the strong positive anomalies of the TP heat source at  $78^{\circ}$ – $95^{\circ}\text{E}$  (Fig. 4b), indicating that the strong TP heat sources cause the strong ascending motions in this region, and are conducive to maintaining the ascending motions and divergence of the upper tropospheric, resulting in the stronger SAH. Meanwhile, there are also positive vertical velocity anomalies over the west Pacific east of  $123^{\circ}\text{E}$  (Fig. 8f), which are located north of  $27^{\circ}\text{N}$  (due to the

location of the cross section in  $22^{\circ}$ – $27^{\circ}\text{N}$ ). Generally, in the middle and upper troposphere, there are strong descending motions on the south side of the WPSH ridge, ascending motions on the north side and near the ridge, and descending motions near the ridge in the lower troposphere. From Fig. 7b, it can be seen that the ridge of the WPAH is located near  $25^{\circ}\text{N}$  in the heat wave high-occurrence years of eastern China. The positive vertical velocity anomaly east of  $23^{\circ}\text{E}$  shown in Fig. 8f is located on the north side of the ridge of WPSH. Therefore, the positive vertical velocity anomalies near the ridge and north side strengthen the descending motion on the south side of the WPSH ridge, which strengthens the development of the WPSH. As a result, strong negative vertical velocity anomalies occur over eastern China (Fig. 8f), which causes the region to be controlled by strong descending motions, resulting in frequent heat waves.

The distribution of specific humidity anomalies corresponds well with the distribution of vertical velocity anomalies (Figs. 8e–h); specific humidity is increased in areas with ascending motions but decreased in regions with descending motion. The maximum positive specific humidity anomalies on the TP occur near the surface at  $85^{\circ}$ – $100^{\circ}\text{E}$  due to the variation in water vapor near the surface (Fig. 8g), corresponding to negative vertical velocity anomalies over the TP that can bring more

TABLE 3. Correlations of the detrended AHS and three components over the TP with the detrended westerly intensity in summer during 1980–2020. Two asterisks (\*\*) indicate the correlation is significant at the 90% confidence level.

	AHS	Local time derivative of temperature	Vertical diabatic heating	Temperature advection
Westerly intensity	−0.139	−0.169	−0.149	0.390**

energy to the atmosphere. While negative specific humidity anomalies exist in high layers above 700 hPa and near the surface in eastern China (Fig. 8h), where strong negative vertical velocity anomalies occur, the drier atmosphere indicates lower precipitation in this region, which is favorable to the occurrence and maintenance of heat waves.

Heat waves in eastern China are mainly influenced by the WPSH and SAH, while the heat waves in northwest China may be influenced by other factors.

*b. The effect of TP heat source on the formation of heat waves in northwest China*

The subtropical westerly jet is divided into two branches due to the blocking of the TP, and the northern branch is located over northwest China, so we will discuss the relationship of the TP heat source with westerlies and of the westerlies with heat waves in northwest China. As shown in Fig. S5a, the intensity of westerly at 200 hPa has weakened by 2–3 m s<sup>−1</sup> during the past 41 years, and is negatively correlated with the AHS over the TP, and the correlation of the detrended AHS over the TP with the detrended westerly intensity are also negative (Table 3), indicating that the TP heat source can affect the intensity of westerlies.

Figure 9 shows that the correlation coefficients between the detrended intensity of westerlies and the detrended number of heat wave days in northwest China are significantly negative. The correlation coefficients are less than −0.4 in the eastern Tarim Basin, western Inner Mongolia, and Junggar Basin, where heat waves are more frequent, which is basically same as those without detrending (Fig. S5b). This indicates that the intensity of westerlies is connected with heat waves in northwest China, and the weakening of the westerly is favorable to the occurrence of heat waves in northwest China.

The correlation between the intensity of westerlies and the three components of the AHS over the TP is shown in Table S1. The intensity of westerlies is negatively correlated with vertical diabatic heating, while it is positively correlated with temperature advection; the correlation of the detrended vertical diabatic heating over the TP with the detrended westerly intensity are also negative, and the detrended temperature advection over the TP is still positively correlated with detrended westerly intensity (Table 3). Kuang et al. (2007) found that diabatic heating at the upper and middle troposphere over the TP can affect the intensity and shift of the westerly jet during June–July. The meridional temperature difference caused by the horizontal temperature advection of heat source is the main factor determining the meridional shift of the westerly jet. Sato and Kimura (2005) also found that the diabatic heating over the TP becomes much stronger from June to September, causing the subtropical westerly jet to retreat poleward. The northward shift of the westerly jet in summer strengthens the westerly intensity at

high latitudes and weakens it at middle and low latitudes (Nan et al. 2021). These results indicate that stronger vertical heating and weaker temperature advection over the TP lead to weaker westerlies, which is conducive to the formation and maintenance of anticyclones, resulting in frequent heat waves in northwest China.

For the heat wave high-occurrence years of northwest China, the WPSH and SAH also exist (Figs. 10a,d). However, the intensity and area of the SAH at 200 hPa in the heat wave high-occurrence years of northwest China are significantly smaller than those in eastern China. The west extending point of the WPSH is farther eastward. The geopotential height anomalies in the heat wave anomalous years of northwest China show a “negative–positive–negative” pattern from northwest to southeast (Figs. 10d–f), with the strongest anomalous anticyclone over northwest China and the Mongolian Plateau, especially at 200 hPa. The anomalous high pressure (anticyclone) extends vertically from near the surface to high levels, with a strong and a weak anomalous low pressure on its left side and right side, respectively, forming “omega” patterns. The low pressures on both sides of the anomalous high pressure help keep the high pressure stationary (Dole and Gordon 1983; Degirmendžić and Wibig 2007).

The wind field anomalies are also larger in the heat wave high-occurrence years of northwest China than in eastern China (figure omitted), especially at 200 and 500 hPa. The wind speed anomalies are negative over the whole westerly belt at 30°–50°N at 200 hPa. The negative anomalies at 200 hPa are mainly at

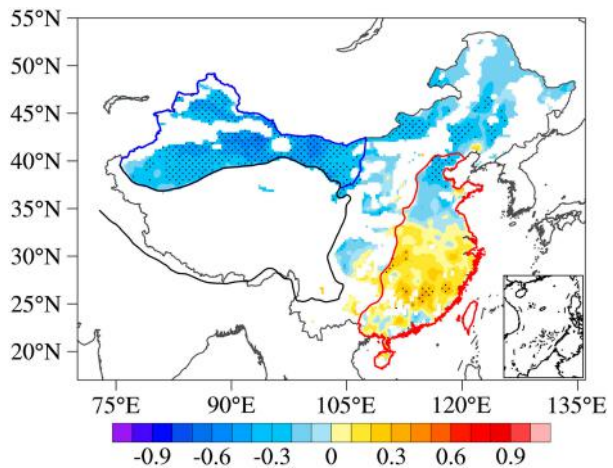


FIG. 9. Correlation of the westerly intensity with the number of heat wave days in summer during 1980–2020. The black dotted areas indicate that the correlations are significant at the 90% confidence level. The red and blue curves denote the zones of eastern China and northwest China, respectively. The black curve is the contour at an altitude of 2000 m, which indicates the TP.

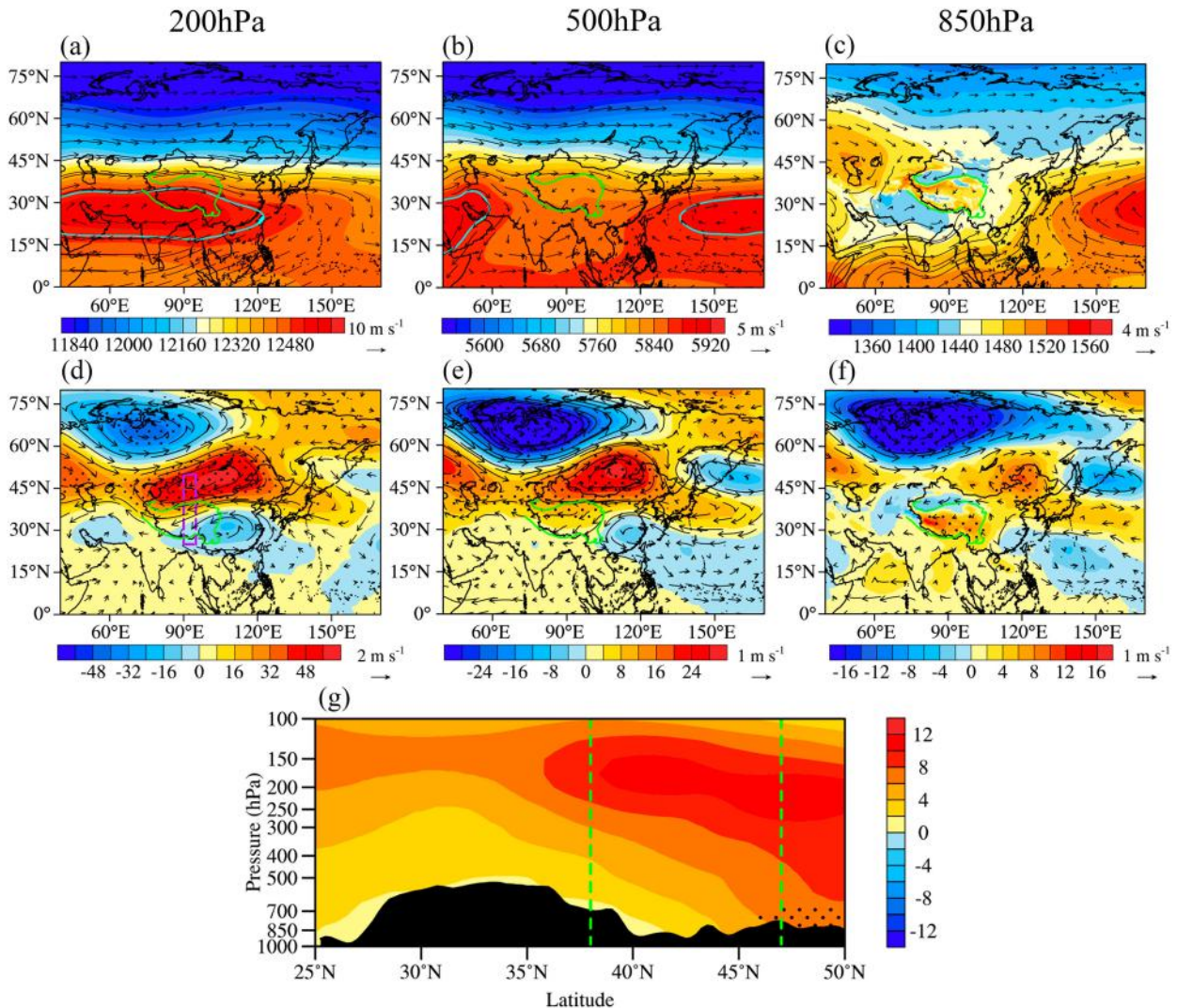


FIG. 10. Mean summer geopotential height fields (color; unit: gpm) and horizontal wind fields (vectors; unit:  $\text{m s}^{-1}$ ) of (a) 200, (b) 500, and (c) 850 hPa in the summer of heat wave high-occurrence years of northwest China and (d)–(f) the anomalies of geopotential height (color; unit: gpm) and horizontal wind fields (vectors; unit:  $\text{m s}^{-1}$ ) between the heat wave high-occurrence years and low-occurrence years during 1980–2020. The blue curves in (a) and (b) are the contours at 12500 and 5880 gpm, respectively. The green curves are the contours at an altitude of 2000 m, which represent the TP. The purple dashed box in (d) indicates the location of the cross section of the anomalies of the mean geopotential height field in (g). (g) The cross section of the anomalies in the mean geopotential height field at 83°–90°E between the heat wave high-occurrence years and low-occurrence years. The black shading indicates topography. The dashed green lines indicate the location of northwest China. The black dotted areas in (d)–(g) indicate that the anomalies are significant at the 90% confidence level.

80°–120°E and are more than  $8 \text{ m s}^{-1}$ . The negative anomalies of the wind field at 200 hPa in eastern China are mainly at 30°–45°N, 80°–135°E and 45°–60°N, 40°–80°E and the intensity of negative anomalies is only half of that in heat wave anomalous years of northwest China, suggesting that the mechanisms affecting heat waves in the two regions may be different.

From the meridional cross section of mean geopotential height anomalies (Fig. 10g), a strong anomalous high pressure near 200 hPa exists over the northern slope of the TP and the Tarim Basin. The anticyclone (high pressure system) from 200 to 500 hPa is a stationary and persistent weather pattern,

which means the weather will mainly remain dry and stabilize in a few days or weeks under the high pressure system. The region controlled by the anticyclone is dominated by descending motions, which encounter the northern slope of the TP and the Tianshan Mountains will be further strengthened by the effects of downslope topography, forming a warm low pressure in northwest China and blowing dry and hot easterly winds (Fig. 10c), thereby resulting in heat waves.

Meanwhile, the diabatic heating over the TP can initiate Rossby wave, with the upper tropospheric subtropical westerly jet retreating northward during summer, Rossby waves

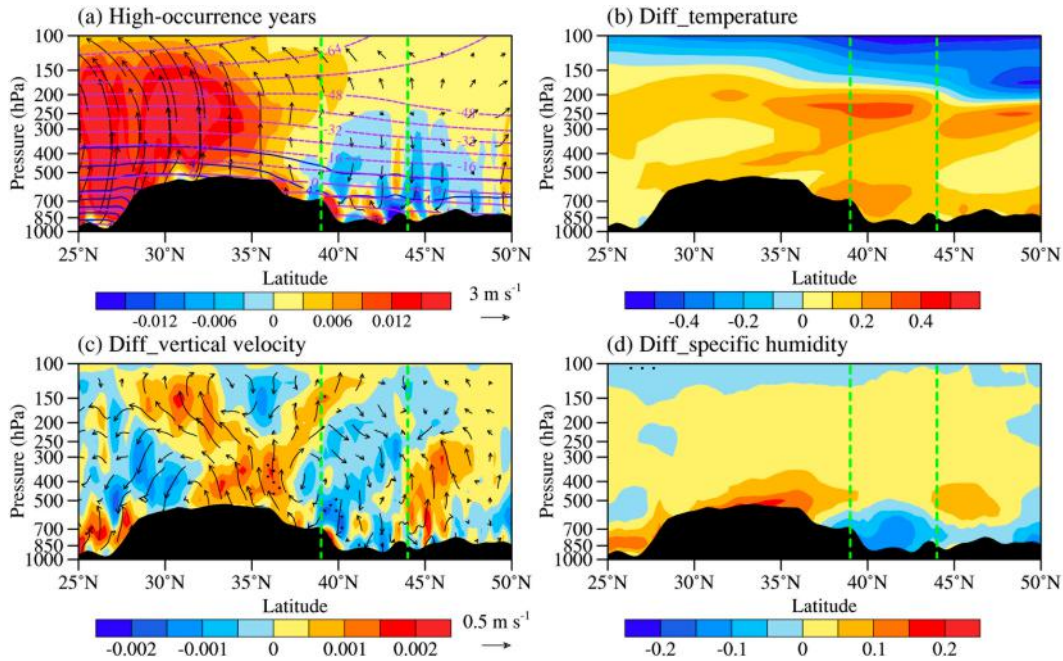


FIG. 11. (a) Cross section of the mean temperature (purple contours; unit:  $^{\circ}\text{C}$ ), vertical velocity (color; unit:  $\text{m s}^{-1}$ ; positive values indicate ascending motion), wind field (vectors of  $u$  and  $w$   $\times$  300; unit:  $\text{m s}^{-1}$ ) and specific humidity (blue contours; unit:  $\text{g kg}^{-1}$ ) at  $90^{\circ}$ – $95^{\circ}\text{E}$  in the summer of heat wave high-occurrence years of northwest China and (b)–(d) the anomalies between the heat wave high-occurrence years and low-occurrence years. The black shading indicates topography. The dashed green lines indicate the location of northwest China. The black dotted areas in (b)–(d) indicate that the anomalies are significant at the 90% confidence level.

can propagate northward on the north of the TP and then form an almost stationary state, resulting in descending motion over the north of the TP (Sato and Kimura 2005; Hoskins 1996), which favors the appearance of heat waves in northwest China.

From the meridional cross section of the mean vertical velocity, wind field, temperature, and specific humidity at  $83^{\circ}$ – $90^{\circ}\text{E}$  (see Fig. 3b) in the heat wave high-occurrence years of northwest China (Fig. 11a), strong ascending motions exist over the TP, with the strongest over the southern slope of the TP. There are descending motions over the Tarim Basin and Turpan Basin, with stronger ascending motion anomalies over the TP and descending motion anomalies over northwest China in the heat wave high-occurrence years of northwest China (Fig. 11c). Positive temperature anomalies exist near the surface in the Tarim Basin and Turpan Basin, suggesting the high occurrence of heat waves (Fig. 11b). Over the northern TP and the Tarim Basin, there are also positive temperature anomalies from 400 to 200 hPa, and the center of the positive anomalies is located at approximately 250 hPa over the Tarim Basin. Combined with Fig. 11g, this indicates that a strong anomalous warm high pressure exists over northwest China during the heat wave high-occurrence years. According to the thermal wind principle, the variation in the westerlies at 200 hPa is mainly modulated by the temperature gradient caused by TP heating (Krishnamurti 1961; Schiemann et al. 2009). The existence of anomalous warm high pressure over the Tarim Basin reduces the meridional temperature gradient

over northwest China and the TP, causing the westerlies to weaken. The specific humidity in the heat wave anomalous years of northwest China shows positive anomalies near the surface of the TP (Fig. 11d) and is stronger than that in the heat wave anomalous years of eastern China. The negative specific humidity anomalies near the surface of Tarim Basin and Turpan Basin, although not significant, could partly contribute to maintain heat waves in northwest China.

## 6. Discussion and conclusions

### a. Discussion

Based on correlation analysis and composite analysis, we consider that the AHS over the TP can influence the heat waves in eastern China through WPSH and SAH and influence the heat waves in northwest China through westerlies.

According to the results after detrending, the correlations between TP heat source and heat waves in China are decreased, and so are the correlations between TP heat source and indices of both WPSH and SAH, which indicates that some of the correlations are contributed by the linear trend, which is mainly caused by global warming or lower-boundary forcing. Besides, the interannual variability is generally due to atmospheric internal variability. Here, we consider that the relations of the strengthening of TP heat source and the increase in heat waves in China after detrending are due to the atmospheric internal variability. As He et al. (2023) reported, a significant anomalous

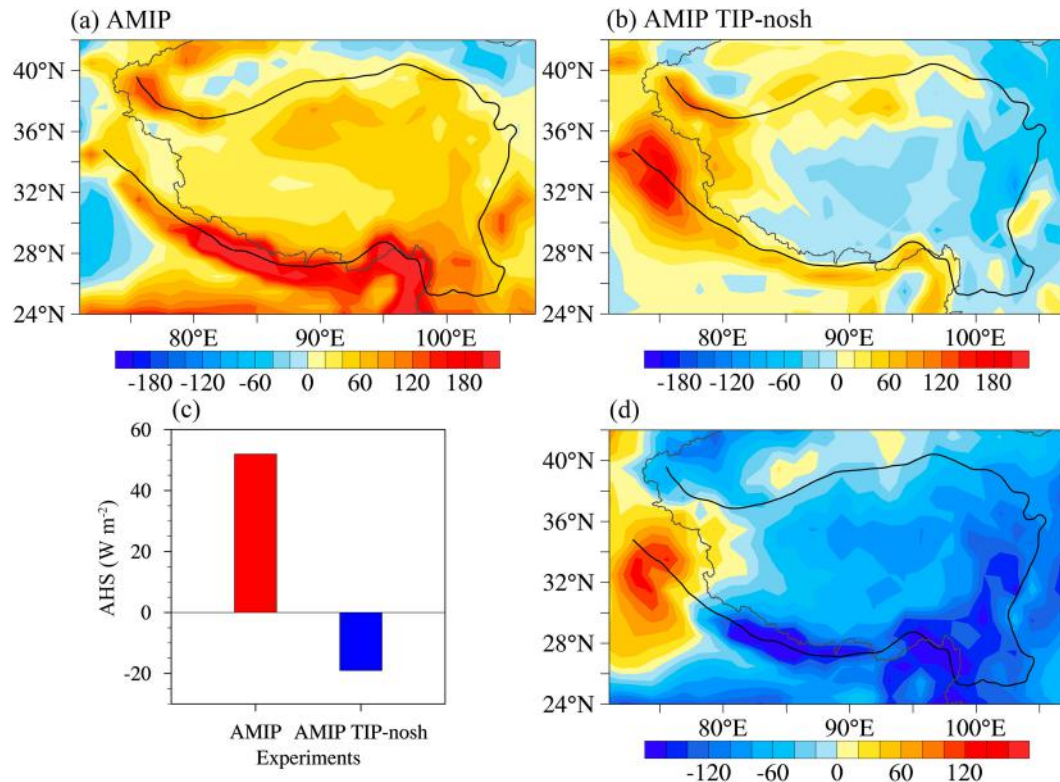


FIG. 12. Spatial distribution of long-term means of the AHS over the TP from the (a) AMIP experiment (unit:  $\text{W m}^{-2}$ ) and (b) AMIP TIP-nosh experiment (unit:  $\text{W m}^{-2}$ ) in summer during 1980–2020. (c) Regional average of the AHS over the TP from the AMIP experiment and AMIP TIP-nosh experiment (unit:  $\text{W m}^{-2}$ ). (d) Spatial distribution of the difference in the AHS over the TP from the AMIP experiment and AMIP TIP-nosh experiment (unit:  $\text{W m}^{-2}$ ). The black curve is the contour at an altitude of 2000 m, which indicates the TP.

anticyclone located over the north TP was found during the 2022 summer heat wave in eastern China, and they concluded that the anomalous anticyclone is a part of the wave train at midlatitudes and can be considered as an atmospheric internal variability. The anomalous anticyclones over the north and northeast TP during the heat wave anomalous years in eastern and northwest China are also found in Figs. 8 and 11, and these two anomalous anticyclones are also part of the Rossby wave train propagating along different directions, which can also be considered as caused by the atmospheric internal variability. Many studies have revealed the essential role of the midlatitude wave train in the heat waves over eastern China (W. Wang et al. 2013, 2014; Chen and Zhou 2018; Gao et al. 2018), revealing the impact of atmospheric internal variability.

In addition, He et al. (2023) suggested that the anomalous easterlies over the TP during the 2022 summer are due to the synergistic effects of internal atmospheric variability and anomalous sea surface temperatures, which contributed about 2/3 and 1/3, respectively. It has also been suggested that current anthropogenic influences are not enough to exceed the impact of natural variability patterns on heat wave trends at most subcontinental scales (Brown et al. 2008). These studies conclude that for the variation of heat waves, the contribution of interannual variation is greater than the linear trend.

Furthermore, we verify the above results by two sets of experiments from phase 6 of the Coupled Model Intercomparison Project (CMIP6). The experiment of the Atmospheric Model Intercomparison Project (AMIP) simulation of CMIP6 is used as a reference experiment (AMIP experiment; He et al. 2019). One of the CMIP6 Global Monsoons Model Intercomparison Project (GMMIP) Tier-3 experiments is used as a sensitivity experiment (AMIP-TIP-nosh experiment; He et al. 2020). In the AMIP-TIP-nosh experiment, the vertical temperature diffusion term in the atmospheric thermodynamic equation, which is equivalent to the vertical diabatic heating, is set to zero where topographies are above 500 m in the mainland of Asia. Other detailed model settings are given in the supplemental material.

As indicated in Fig. 12a, in the AMIP experiment, the TP is shown to be a heat source in summer, and the high value area of the AHS is mainly distributed in the south edge of the TP, the eastern TP is also shown to be a strong heat source, which is basically consistent with the distribution of Fig. 2a. The values of AHS calculated by the AMIP experiment are lower than that calculated by ERA5, which is due to the fact that the resolution of the vertical layers from 1000 to 100 hPa in the AMIP experiment is lower than that of ERA5 data, making the calculation smaller after integration in the vertical

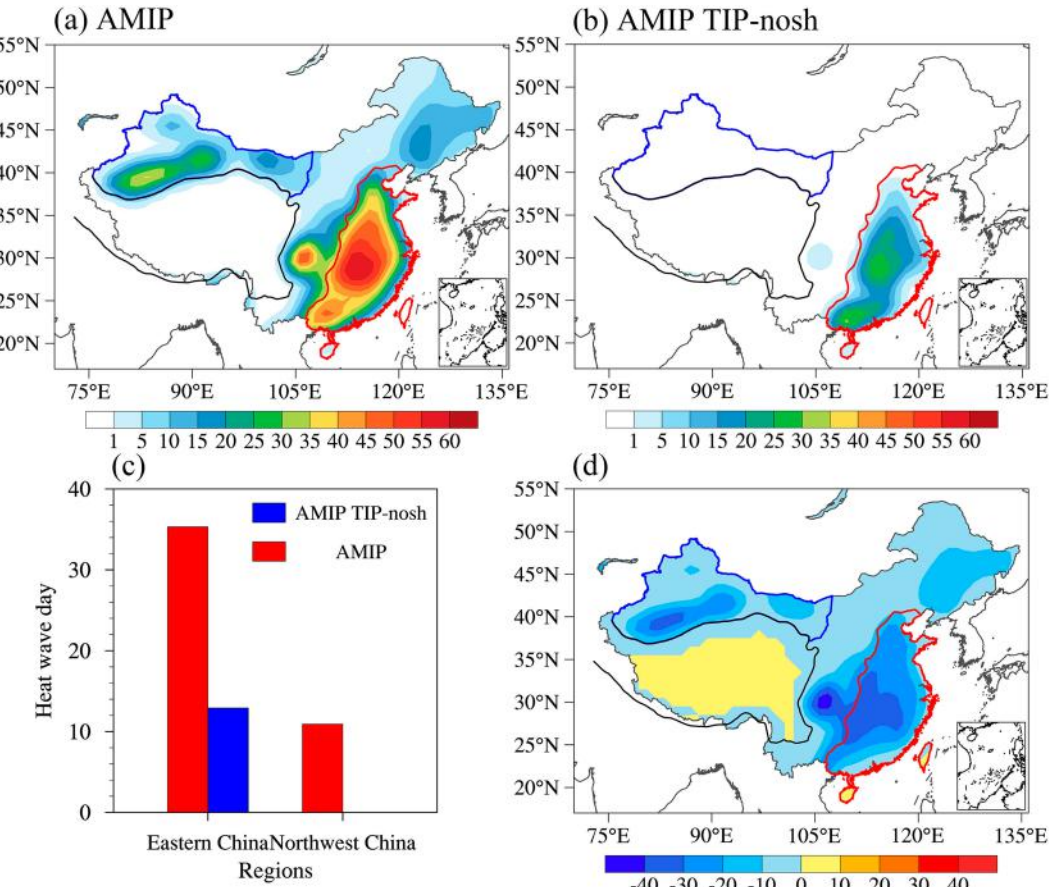


FIG. 13. Spatial distribution of long-term means number of heat wave days from the (a) AMIP experiment (unit: days) and (b) AMIP TIP-nosh experiment (unit: days) in summer during 1980–2020. (c) Regional average of the heat wave days of eastern China and northwest China from the AMIP experiment and AMIP TIP-nosh experiment (unit: days). (d) Spatial distribution of the difference in the heat wave days from AMIP experiment and AMIP TIP-nosh experiment (unit: days). The red and blue curves denote the zones of eastern China and northwest China, respectively. The black curve is the contour at an altitude of 2000 m, which indicates the TP.

direction. From the spatial distribution of AHS over the TP, we regard the simulation results as basically reasonable. In the AMIP TIP-nosh experiment (Fig. 12b), when the vertical diabatic heating term in the atmospheric thermodynamic equation is set to zero in the specified region, except for the western TP and north edge of the TP, the rest of TP is shown to be a cold source in summer. It also indicates the dominance of vertical diabatic heating in the three components of the AHS over the TP. From the differences between the two sets of experiments (Fig. 12d), the areas with the largest differences are mainly located in the southern and eastern TP, which are the areas with stronger AHS over the TP. For the regional average, the AHS over the TP is reduced by 136.62% after the vertical diabatic heating is set to zero (Fig. 12c).

We calculated the heat wave days from the AMIP experiment, as shown in Fig. 13. The spatial distribution of heat wave days in China from the AMIP experiment is similar to that from the ERA5 data, which also shows that heat waves occur mainly in northwest China, eastern China, and the Sichuan basin (Fig. 13a). The number of heat wave days simulated

by the AMIP experiment in northwest China is basically consistent with that from the ERA5 data, while the AMIP experiment has significantly overestimated the heat wave days in eastern China. For the trend of heat wave days, the results of the AMIP experiment are similar to that from ERA5 (not shown), with increasing trends and comparable rates in northwest China, eastern China, and the Sichuan basin. On the whole, the results under AMIP experiment can reflect the characteristics of heat waves in China to some extent. In the AMIP TIP-nosh experiment (Fig. 13b), the number of heat wave days decreases significantly in eastern China, while no heat wave is simulated in northwest China. Comparing the differences between two sets of experiments, it is found that the more heat waves are simulated in the AMIP experiment, the more heat waves are reduced in the AMIP TIP-nosh experiment (Fig. 13d). For the regional average (Fig. 13c), the heat wave days in Eastern China are reduced by 63.44% in the AMIP TIP-nosh experiment compared with the results of AMIP experiment, while no heat waves are simulated in northwest China in the AMIP TIP-nosh experiment.

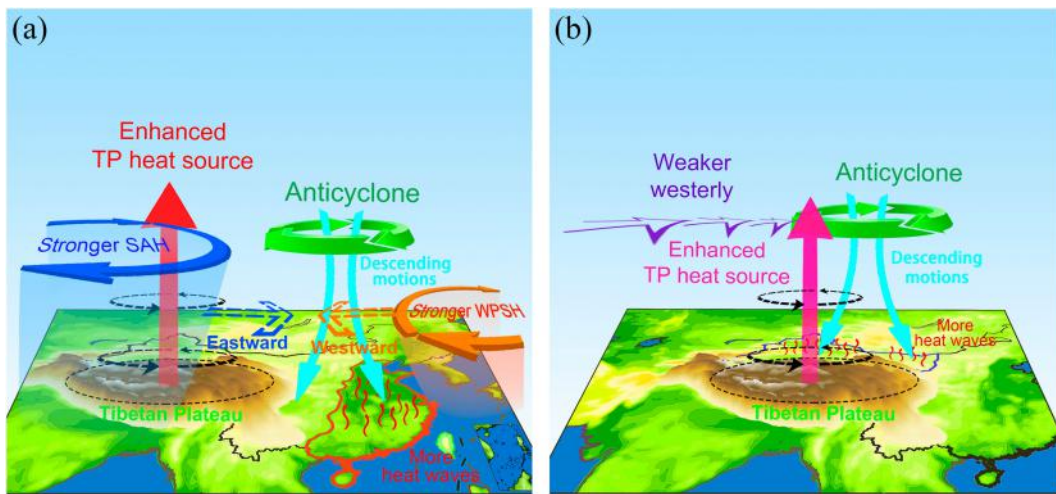


FIG. 14. Mechanisms of the TP heat source influencing heat waves in (a) eastern China and (b) northwest China. The thick red arrow in (a) and the thin violet-red arrow in (b) indicate the enhanced TP heat source affecting heat wave in eastern China is stronger than that in northwest China.

Although there are some biases in the CMIP experiments, and the range where the vertical diabatic heating sets to zero in AMIP-TIP-nosh experiment is wider, we can still qualitatively find the association between the AHS over the TP and the heat wave days in China.

In the background of recent trend of heat wave in eastern and northwest China, it seems worthwhile to discuss potential future changes of heat waves. We use the output of the medium-resolution Beijing Climate Center Climate System Model, version 2 (BCC-CSM2-MR), from CMIP6 to discuss future changes in the number of heat wave days in eastern and northwest China under different Shared Socioeconomic Pathway (SSP) scenarios (see the online supplemental material for detailed model settings). As shown in Fig. S7, compared with ERA5, the BCC-CSM2-MR model also overestimates the number of heat wave days in eastern China under the historical scenario, but the simulation of heat wave days in northwest China is relatively good (Fig. S7a). The BCC-CSM2-MR model can simulate the increasing trend of heat wave days in eastern and northwest China, the distribution of the trend is similar to that of ERA5 (Fig. S7e), and the simulation effect is generally reliable.

Under the scenarios of SSP1-2.6, SSP2-4.5, and SSP5-8.5 from the BCC-CSM2-MR mode, the numbers of heat wave days in eastern and northwest China increase with the enhancement of emissions (Figs. S7b–d,i–k). In terms of trends, the heat wave days in the SSP1-2.6 scenario show a significant increasing trend in the North China Plain, the middle and lower reaches of the Yangtze River, and northwest China, with a weak decreasing trend in the southern coastal region (Fig. S7f). In the SSP2-4.5 and SSP5-8.5 scenarios, the number of heat wave days increases significantly throughout eastern and northwest China; the increasing trend in the number of heat wave days in eastern and northwest China is substantially higher than in the SSP1-2.6 scenario, with the high value area of variation of heat wave days shifted southward in eastern China (Figs. S7g,h).

In terms of regional averages, the number of heat wave days in eastern and northwest China tends to increase under all three scenarios, and the increasing trend of heat wave days increases with the enhancement of emissions (Fig. S8). Compared to the historical scenario, the average number of heat wave days in eastern China increases in the future by an average of 83.71%, 95.42%, and 135.67% under the scenarios of SSP1-2.6, SSP2-4.5, and SSP5-8.5, respectively. For northwest China, the average number of heat wave days under SSP1-2.6, SSP2-4.5, and SSP5-8.5 scenarios increased by 94.08%, 163.24%, and 275.26%, respectively (Fig. S8b).

#### b. Conclusions

In summary, during the past 41 years, heat wave days in most regions show increasing tendencies, with rates of 0.09 and 0.24 days  $\text{yr}^{-1}$  in eastern China and northwest China, respectively. Meanwhile, the AHS over the TP is stronger in the eastern and southern TP and shows increasing tendencies that are stronger in the southwestern TP over  $2 \text{ W m}^{-2} \text{ yr}^{-1}$ . The AHS over the TP is positively correlated with heat waves in eastern China and northwest China, and most of the correlation coefficients range from 0.3 to 0.5.

In terms of the mechanisms, for eastern China (Fig. 14a), due to the AHS anomalies over the TP, the anomalous ascending motions caused by the vertical diabatic heating of the TP cause the WPSH and SAH to be stronger and closer. The two high pressure systems form an anomalous anticyclone over northern eastern China, leading the descending motions to control eastern China, which causes more heat waves in eastern China. For northwest China (Fig. 14b), the positive anomalies of AHS over the TP are stronger than those in heat wave anomalous years of eastern China. The stronger vertical diabatic heating and weaker temperature advection over the TP induce a weakened westerly at 200 hPa. The weakened westerly at middle and low latitudes is favorable to the occurrence and maintenance of anticyclones over northwest China.

The descending motions generated by the anticyclone are further intensified by the downslope topography of the northern slopes of the TP and the Tianshan Mountains, which induces more frequent heat waves in northwest China.

In summary, the mechanisms of the AHS over the TP affecting heat waves in eastern China and northwest China are different. On the one hand, the AHS over the TP affects the heat waves in eastern and northwest China through different weather systems, with the AHS over the TP affecting the heat waves in eastern China by influencing the WPSH and SAH, and affecting the heat waves in northwest China by influencing the westerlies. On the other hand, the AHS over the TP triggers wave trains eastward and northward to affect the corresponding weather systems and heat waves in the two regions, respectively.

The factors affecting heat waves also include global warming and lower boundary forcing which contribute to the linear trend, such as sea surface temperature anomalies, ice area variations in the Arctic Ocean, and soil moisture anomalies or urbanization. The Arctic sea ice loss under a warming climate will induce more frequent quasi-barotropic ridges, which may lead to more heat waves over western North America (Wang et al. 2022). The sea ice concentration in the Barents–Kara Sea can influence the spatial distribution of heat waves in North China by modulating atmospheric circulation (Zhang et al. 2022). Stronger heat waves occur over western Russia if sea surface temperatures are anomalously warm in the Barents Sea and the Arabian Sea, as a result of the dynamic response of the atmosphere (Sedláček et al. 2011). Drier land surface conditions can amplify heat waves in Europe through the feedback of atmospheric circulation (Merrifield et al. 2019).

Our research shows that TP heat sources have a close association with heat waves in the surrounding areas. Due to the high sensitivity of the TP to climate change, we need to give more attention to the relationship between the TP and surrounding heat waves. In this paper, we investigate the associations between the two by using data analysis, and we will use a numerical model to quantify the contribution of TP heat sources affecting heat waves in the surrounding area due to linear trend and interannual variability in future research.

**Acknowledgments.** This research was mainly supported by the National Natural Science Foundation of China (91937302 and 41991231), and the Fundamental Research Funds for the Central Universities (Izujbky-2022-kb11). Most importantly, with the reviewers' constructive comments and elaborate feedback, our paper has been greatly improved. We are extremely grateful to the reviewers for giving time and expertise to review our paper.

**Data availability statement.** The ERA5 data were downloaded from the European Centre for Medium-Range Weather Forecasts (ECMWF) at the Climate Data Store (<https://cds.climate.copernicus.eu/cdsapp#!/home>). The CMIP6 data were downloaded from the WCRP Coupled Model Intercomparison Project (phase 6) (<https://esgf-node.llnl.gov/projects/cmip6/>).

## REFERENCES

Adélaïde, L., O. Chanel, and M. Pascal, 2022: Health effects from heat waves in France: An economic evaluation. *Eur. J. Health Econ.*, **23**, 119–131, <https://doi.org/10.1007/s10198-021-01357-2>.

Andersen, O. B., S. I. Seneviratne, J. Hinderer, and P. Viterbo, 2005: GRACE-derived terrestrial water storage depletion associated with the 2003 European heat wave. *Geophys. Res. Lett.*, **32**, L18405, <https://doi.org/10.1029/2005GL023574>.

Anderson, G. B., and M. L. Bell, 2011: Heat waves in the United States: Mortality risk during heat waves and effect modification by heat wave characteristics in 43 U.S. communities. *Environ. Health Perspect.*, **119**, 210–218, <https://doi.org/10.1289/ehp.1002313>.

Barriopedro, D., E. M. Fischer, J. Luterbacher, R. M. Trigo, and R. García-Herrera, 2011: The hot summer of 2010: Redrawing the temperature record map of Europe. *Science*, **332**, 220–224, <https://doi.org/10.1126/science.1201224>.

Black, E., and R. Sutton, 2007: The influence of oceanic conditions on the hot European summer of 2003. *Climate Dyn.*, **28**, 53–66, <https://doi.org/10.1007/s00382-006-0179-8>.

Brás, T. A., J. Seixas, N. Carvalhais, and J. Jägermeyr, 2021: Severity of drought and heatwave crop losses tripled over the last five decades in Europe. *Environ. Res. Lett.*, **16**, 065012, <https://doi.org/10.1088/1748-9326/abf004>.

Brown, S. J., J. Caesar, and C. A. T. Ferro, 2008: Global changes in extreme daily temperature since 1950. *J. Geophys. Res.*, **113**, D05115, <https://doi.org/10.1029/2006JD008091>.

Brunner, L., G. C. Hegerl, and A. K. Steiner, 2017: Connecting atmospheric blocking to European temperature extremes in spring. *J. Climate*, **30**, 585–594, <https://doi.org/10.1175/JCLI-D-16-0518.1>.

Bustan, A., M. Sagi, Y. De Malach, and D. Pasternak, 2004: Effects of saline irrigation water and heat waves on potato production in an arid environment. *Field Crops Res.*, **90**, 275–285, <https://doi.org/10.1016/j.fcr.2004.03.007>.

Cerne, S. B., and C. S. Vera, 2011: Influence of the intraseasonal variability on heat waves in subtropical South America. *Climate Dyn.*, **36**, 2265–2277, <https://doi.org/10.1007/s00382-010-0812-4>.

Chan, S. C., and S. Nigam, 2009: Residual diagnosis of diabatic heating from ERA-40 and NCEP reanalyses: Intercomparisons with TRMM. *J. Climate*, **22**, 414–428, <https://doi.org/10.1175/2008JCLI2417.1>.

Chang, E. K. M., 2009: Diabatic and orographic forcing of northern winter stationary waves and storm tracks. *J. Climate*, **22**, 670–688, <https://doi.org/10.1175/2008JCLI2403.1>.

Chen, R., and R. Lu, 2015: Comparisons of the circulation anomalies associated with extreme heat weather in different regions in eastern China. *J. Climate*, **28**, 5830–5844, <https://doi.org/10.1175/JCLI-D-14-00818.1>.

Chen, X., and T. Zhou, 2018: Relative contributions of external SST forcing and internal atmospheric variability to July–August heat waves over the Yangtze River valley. *Climate Dyn.*, **51**, 4403–4419, <https://doi.org/10.1007/s00382-017-3871-y>.

Ciais, P., and Coauthors, 2005: Europe-wide reduction in primary productivity caused by the heat and drought in 2003. *Nature*, **437**, 529–533, <https://doi.org/10.1038/nature03972>.

Coumou, D., and S. Rahmstorf, 2012: A decade of weather extremes. *Nat. Climate Change*, **2**, 491–496, <https://doi.org/10.1038/nclimate1452>.

Cowan, T., A. Purich, S. Perkins, A. Pezza, G. Boschat, and K. Sadler, 2014: More frequent, longer, and hotter heat waves

for Australia in the twenty-first century. *J. Climate*, **27**, 5851–5871, <https://doi.org/10.1175/JCLI-D-14-00092.1>.

Degirmendžić, J., and J. Wibig, 2007: Jet stream patterns over Europe in the period 1950–2001—Classification and basic statistical properties. *Theor. Appl. Climatol.*, **88**, 149–167, <https://doi.org/10.1007/s00704-006-0237-5>.

Ding, Q., and B. Wang, 2005: Circumglobal teleconnection in the Northern Hemisphere summer. *J. Climate*, **18**, 3483–3505, <https://doi.org/10.1175/JCLI3473.1>.

Ding, T., W. Qian, and Z. Yan, 2010: Changes in hot days and heat waves in China during 1961–2007. *Int. J. Climatol.*, **30**, 1452–1462, <https://doi.org/10.1002/joc.1989>.

Dole, R. M., and N. D. Gordon, 1983: Persistent anomalies of the extratropical Northern Hemisphere wintertime circulation: Geographical distribution and regional persistence characteristics. *Mon. Wea. Rev.*, **111**, 1567–1586, [https://doi.org/10.1175/1520-0493\(1983\)111,1567:PAOTEN.2.0.CO;2](https://doi.org/10.1175/1520-0493(1983)111,1567:PAOTEN.2.0.CO;2).

—, and Coauthors, 2011: Was there a basis for anticipating the 2010 Russian heat wave? *Geophys. Res. Lett.*, **38**, L06702, <https://doi.org/10.1029/2010GL046582>.

Duan, A., G. Wu, Q. Zhang, and Y. Liu, 2006: New proofs of the recent climate warming over the Tibetan Plateau as a result of the increasing greenhouse gases emissions. *Chin. Sci. Bull.*, **51**, 1396–1400, <https://doi.org/10.1007/s11434-006-1396-6>.

—, M.-R. Wang, and Z.-X. Xiao, 2014: Uncertainties in quantitatively estimating the atmospheric heat source over the Tibetan Plateau. *Atmos. Ocean. Sci. Lett.*, **7**, 28–33, <https://doi.org/10.1080/16742834.2014.1144713>.

Fischer, E. M., S. I. Seneviratne, P. L. Vidale, D. Lüthi, and C. Schär, 2007: Soil moisture–atmosphere interactions during the 2003 European summer heat wave. *J. Climate*, **20**, 5081–5099, <https://doi.org/10.1175/JCLI4288.1>.

Gao, M., B. Wang, J. Yang, and W. Dong, 2018: Are peak summer sultry heat wave days over the Yangtze–Huaihe River basin predictable? *J. Climate*, **31**, 2185–2196, <https://doi.org/10.1175/JCLI-D-17-0342.1>.

Ge, J., Q. You, and Y. Zhang, 2019: Effect of Tibetan Plateau heating on summer extreme precipitation in eastern China. *Atmos. Res.*, **218**, 364–371, <https://doi.org/10.1016/j.atmosres.2018.12.018>.

He, B., and Coauthors, 2019: CAS FGOALS-f3-L model datasets for CMIP6 historical Atmospheric Model Intercomparison Project simulation. *Adv. Atmos. Sci.*, **36**, 771–778, <https://doi.org/10.1007/s00376-019-9027-8>.

—, and Coauthors, 2020: CAS FGOALS-f3-L model datasets for CMIP6 GMMIP Tier-1 and Tier-3 experiments. *Adv. Atmos. Sci.*, **37**, 18–28, <https://doi.org/10.1007/s00376-019-9085-y>.

He, C., T. Zhou, L. Zhang, X. Chen, and W. Zhang, 2023: Extremely hot East Asia and flooding western South Asia in the summer of 2022 tied to reversed flow over Tibetan Plateau. *Climate Dyn.*, **61**, 2103–2119, <https://doi.org/10.1007/s00382-023-06669-y>.

He, H., J. W. McGinnis, Z. Song, and M. Yanai, 1987: Onset of the Asian summer monsoon in 1979 and the effect of the Tibetan Plateau. *Mon. Wea. Rev.*, **115**, 1966–1995, [https://doi.org/10.1175/1520-0493\(1987\)115<1966:OOTASM>2.0.CO;2](https://doi.org/10.1175/1520-0493(1987)115<1966:OOTASM>2.0.CO;2).

Held, I. M., M. Ting, and H. Wang, 2002: Northern winter stationary waves: Theory and modeling. *J. Climate*, **15**, 2125–2144, [https://doi.org/10.1175/1520-0442\(2002\)015<2125:NWSWTA>2.0.CO;2](https://doi.org/10.1175/1520-0442(2002)015<2125:NWSWTA>2.0.CO;2).

Hersbach, H., and Coauthors, 2019a: ERA5 monthly averaged data on pressure levels from 1940 to present. Copernicus Climate Change Service (C3S) Climate Data Store (CDS), accessed 9 May 2021, <https://doi.org/10.24381/cds.6860a573>.

—, and Coauthors, 2019b: ERA5 monthly averaged data on single levels from 1940 to present. Copernicus Climate Change Service (C3S) Climate Data Store (CDS), accessed 9 January 2021, <https://doi.org/10.24381/cds.f17050d7>.

—, and Coauthors, 2020: The ERA5 global reanalysis. *Quart. J. Roy. Meteor. Soc.*, **146**, 1999–2049, <https://doi.org/10.1002/qj.3803>.

Hoskins, B. J., 1996: On the existence and strength of the summer subtropical anticyclones. *Bull. Amer. Meteor. Soc.*, **77**, 1287–1292.

Hu, K., G. Huang, and R. Huang, 2011: The impact of tropical Indian Ocean variability on summer surface air temperature in China. *J. Climate*, **24**, 5365–5377, <https://doi.org/10.1175/2011JCLI4152.1>.

Jiménez-Esteve, B., and D. I. V. Domeisen, 2022: The role of atmospheric dynamics and large-scale topography in driving heatwaves. *Quart. J. Roy. Meteor. Soc.*, **148**, 2344–2367, <https://doi.org/10.1002/qj.4306>.

Krishnamurti, T. N., 1961: The subtropical jet stream of winter. *J. Atmos. Sci.*, **18**, 172–191, [https://doi.org/10.1175/1520-0469\(1961\)018%3C0172:TSJSOW%3E2.0.CO;2](https://doi.org/10.1175/1520-0469(1961)018%3C0172:TSJSOW%3E2.0.CO;2).

Kuang, X., Y. Zhang, and J. Liu, 2007: Seasonal variations of the East Asian subtropical westerly jet and the thermal mechanism. *Acta Meteor. Sin.*, **21**, 192–203.

Lau, N.-C., and M. J. Nath, 2012: A model study of heat waves over North America: Meteorological aspects and projections for the twenty-first century. *J. Climate*, **25**, 4761–4784, <https://doi.org/10.1175/JCLI-D-11-00575.1>.

—, and —, 2014: Model simulation and projection of European heat waves in present-day and future climates. *J. Climate*, **27**, 3713–3730, <https://doi.org/10.1175/JCLI-D-13-00284.1>.

Li, N., P. Zhao, J. Wang, and Y. Deng, 2019: Estimation of surface heat fluxes over the central Tibetan Plateau using the maximum entropy production model. *J. Geophys. Res. Atmos.*, **124**, 6827–6840, <https://doi.org/10.1029/2018JD029959>.

Lin, L., E. Ge, X. Liu, W. Liao, and M. Luo, 2018: Urbanization effects on heat waves in Fujian Province, southeast China. *Atmos. Res.*, **210**, 123–132, <https://doi.org/10.1016/j.atmosres.2018.04.011>.

Liu, G., R. Wu, S. Sun, and H. Wang, 2015: Synergistic contribution of precipitation anomalies over northwestern India and the South China Sea to high temperature over the Yangtze River valley. *Adv. Atmos. Sci.*, **32**, 1255–1265, <https://doi.org/10.1007/s00376-015-4280-y>.

Liu, X., and B. Chen, 2000: Climatic warming in the Tibetan Plateau during recent decades. *Int. J. Climatol.*, **20**, 1729–1742, [https://doi.org/10.1002/1097-0088\(20001130\)20:14<1729::AID-JOC556>3.0.CO;2-Y](https://doi.org/10.1002/1097-0088(20001130)20:14<1729::AID-JOC556>3.0.CO;2-Y).

Liu, Y., M. Lu, H. Yang, A. Duan, B. He, S. Yang, and G. Wu, 2020: Land–atmosphere–ocean coupling associated with the Tibetan Plateau and its climate impacts. *Natl. Sci. Rev.*, **7**, 534–552, <https://doi.org/10.1093/nsr/nwaa011>.

Lu, M., S. Yang, C. Zhu, J. Wang, S. Lin, W. Wei, and H. Fan, 2023: Thermal impact of the southern Tibetan Plateau on the Southeast Asian summer monsoon and modulation by the tropical Atlantic SST. *J. Climate*, **36**, 1319–1330, <https://doi.org/10.1175/JCLI-D-22-0493.1>.

Lu, Y., and L. Kueppers, 2015: Increased heat waves with loss of irrigation in the United States. *Environ. Res. Lett.*, **10**, 064010, <https://doi.org/10.1088/1748-9326/10/6/064010>.

Luo, M., and N.-C. Lau, 2017: Heat waves in southern China: Synoptic behavior, long-term change, and urbanization effects. *J. Climate*, **30**, 703–720, <https://doi.org/10.1175/JCLI-D-16-0269.1>.

Lyon, B., 2009: Southern Africa summer drought and heat waves: Observations and coupled model behavior. *J. Climate*, **22**, 6033–6046, <https://doi.org/10.1175/2009JCLI3101.1>.

Meehl, G. A., and C. Tebaldi, 2004: More intense, more frequent, and longer lasting heat waves in the 21st century. *Science*, **305**, 994–997, <https://doi.org/10.1126/science.1098704>.

Merrifield, A. L., I. R. Simpson, K. A. McKinnon, S. Sippel, S.-P. Xie, and C. Deser, 2019: Local and nonlocal land surface influence in European heatwave initial condition ensembles. *Geophys. Res. Lett.*, **46**, 14 082–14 092, <https://doi.org/10.1029/2019GL083945>.

Miller, S., K. Chua, J. Coggins, and H. Mohtadi, 2021: Heat waves, climate change, and economic output. *J. Eur. Econ. Assoc.*, **19**, 2658–2694, <https://doi.org/10.1093/jeea/jvab009>.

Nan, S., P. Zhao, J. Chen, and G. Liu, 2021: Links between the thermal condition of the Tibetan Plateau in summer and atmospheric circulation and climate anomalies over the Eurasian continent. *Atmos. Res.*, **247**, 105212, <https://doi.org/10.1016/j.atmosres.2020.105212>.

Narinesingh, V., J. F. Booth, S. K. Clark, and Y. Ming, 2020: Atmospheric blocking in an aquaplanet and the impact of orography. *Wea. Climate Dyn.*, **1**, 293–311, <https://doi.org/10.5194/wcd-1-293-2020>.

Niu, T., L. Chen, and Z. Zhou, 2004: The characteristics of climate change over the Tibetan Plateau in the last 40 years and the detection of climatic jumps. *Adv. Atmos. Sci.*, **21**, 193–203, <https://doi.org/10.1007/BF02915705>.

Pechan, A., and K. Eisenack, 2014: The impact of heat waves on electricity spot markets. *Energy Econ.*, **43**, 63–71, <https://doi.org/10.1016/j.eneco.2014.02.006>.

Pfahl, S., and H. Wernli, 2012: Quantifying the relevance of atmospheric blocking for co-located temperature extremes in the Northern Hemisphere on (sub-) daily time scales. *Geophys. Res. Lett.*, **39**, L12807, <https://doi.org/10.1029/2012GL052261>.

Reiter, E. R., and D.-Y. Gao, 1982: Heating of the Tibet Plateau and movements of the South Asian high during spring. *Mon. Wea. Rev.*, **110**, 1694–1711, [https://doi.org/10.1175/1520-0493\(1982\)110<1694:HOTTPA>2.0.CO;2](https://doi.org/10.1175/1520-0493(1982)110<1694:HOTTPA>2.0.CO;2).

Ren, G., Z. Guan, X. Shao, and D. Y. Gong, 2011: Changes in climatic extremes over mainland China. *Climate Res.*, **50**, 105–111, <https://doi.org/10.3354/cr01067>.

Robine, J.-M., S. L. K. Cheung, S. Le Roy, H. Van Oyen, C. Griffiths, J.-P. Michel, and F. R. Herrmann, 2008: Death toll exceeded 70,000 in Europe during the summer of 2003. *C. R. Biol.*, **331**, 171–178, <https://doi.org/10.1016/j.crvi.2007.12.001>.

Rohini, P., M. Rajeevan, and A. K. Srivastava, 2016: On the variability and increasing trends of heat waves over India. *Sci. Rep.*, **6**, 26153, <https://doi.org/10.1038/srep26153>.

Sanz-Barbero, B., C. Linares, C. Vives-Cases, J. L. González, J. J. López-Ossorio, and J. Díaz, 2018: Heat wave and the risk of intimate partner violence. *Sci. Total Environ.*, **644**, 413–419, <https://doi.org/10.1016/j.scitotenv.2018.06.368>.

Sato, T., and F. Kimura, 2005: Impact of diabatic heating over the Tibetan Plateau on subsidence over northeast Asian arid region. *Geophys. Res. Lett.*, **32**, L05809, <https://doi.org/10.1029/2004GL022089>.

Schiemann, R., D. Lüthi, and C. Schär, 2009: Seasonality and interannual variability of the westerly jet in the Tibetan Plateau region. *J. Climate*, **22**, 2940–2957, <https://doi.org/10.1175/2008JCLI2625.1>.

Schneidereit, A., S. Schubert, P. Vargin, F. Lunkeit, X. Zhu, D. H. W. Peters, and K. Fraedrich, 2012: Large-scale flow and the long-lasting blocking high over Russia: Summer 2010. *Mon. Wea. Rev.*, **140**, 2967–2981, <https://doi.org/10.1175/MWR-D-11-00249.1>.

Sedláček, J., O. Martius, and R. Knutti, 2011: Influence of sub-tropical and polar sea-surface temperature anomalies on temperatures in Eurasia. *Geophys. Res. Lett.*, **38**, L12803, <https://doi.org/10.1029/2011GL047764>.

Shi, X., J. Chen, and M. Wen, 2019: The relationship between heavy precipitation in the eastern region of China and atmospheric heating anomalies over the Tibetan Plateau and its surrounding areas. *Theor. Appl. Climatol.*, **137**, 2335–2349, <https://doi.org/10.1007/s00704-018-02752-1>.

Smith, T. T., B. F. Zaitchik, and J. M. Gohlke, 2013: Heat waves in the United States: Definitions, patterns and trends. *Climatic Change*, **118**, 811–825, <https://doi.org/10.1007/s10584-012-0659-2>.

Smoyer-Tomic, K. E., R. Kuhn, and A. Hudson, 2003: Heat wave hazards: An overview of heat wave impacts in Canada. *Nat. Hazards*, **28**, 465–486, <https://doi.org/10.1023/A:1022946528157>.

Speirs, J. C., D. F. Steinhoff, H. A. McGowan, D. H. Bromwich, and A. J. Monaghan, 2010: Foehn winds in the McMurdo dry valleys, Antarctica: The origin of extreme warming events. *J. Climate*, **23**, 3577–3598, <https://doi.org/10.1175/2010JCLI3382.1>.

Sun, G., Z. Hu, Y. Ma, Z. Xie, F. Sun, J. Wang, and S. Yang, 2021: Analysis of local land atmosphere coupling characteristics over Tibetan Plateau in the dry and rainy seasons using observational data and ERA5. *Sci. Total Environ.*, **774**, 145138, <https://doi.org/10.1016/j.scitotenv.2021.145138>.

Sun, Y., T. Hu, and X. Zhang, 2018: Substantial increase in heat wave risks in China in a future warmer world. *Earth's Future*, **6**, 1528–1538, <https://doi.org/10.1029/2018EF000963>.

Sutton, R. T., and D. L. R. Hodson, 2005: Atlantic Ocean forcing of North American and European summer climate. *Science*, **309**, 115–118, <https://doi.org/10.1126/science.1109496>.

Tan, J., Y. Zheng, G. Song, L. S. Kalkstein, A. J. Kalkstein, and X. Tang, 2007: Heat wave impacts on mortality in Shanghai, 1998 and 2003. *Int. J. Biometeor.*, **51**, 193–200, <https://doi.org/10.1007/s00484-006-0058-3>.

Tan, Z., Y. Liu, Q. Zhu, and T. Shao, 2021: Impact of massive topography on the dust cycle surrounding the Tibetan Plateau. *Atmos. Environ.*, **264**, 118703, <https://doi.org/10.1016/j.atmosenv.2021.118703>.

Teskey, R., T. Werten, I. Bauweraerts, M. Ameye, M. A. McGuire, and K. Steppe, 2015: Responses of tree species to heat waves and extreme heat events. *Plant Cell Environ.*, **38**, 1699–1712, <https://doi.org/10.1111/pce.12417>.

Teuling, A. J., and Coauthors, 2010: Contrasting response of European forest and grassland energy exchange to heatwaves. *Nat. Geosci.*, **3**, 722–727, <https://doi.org/10.1038/ngeo950>.

Wang, B., Q. Bao, B. Hoskins, G. Wu, and Y. Liu, 2008: Tibetan Plateau warming and precipitation change in East Asia. *Geophys. Res. Lett.*, **35**, L14702, <https://doi.org/10.1029/2008GL034330>.

Wang, H., Y. Gao, Y. Wang, and L. Sheng, 2022: Arctic sea ice modulation of summertime heatwaves over western North America in recent decades. *Environ. Res. Lett.*, **17**, 074015, <https://doi.org/10.1088/1748-9326/ac765a>.

Wang, M., X. Yan, J. Liu, and X. Zhang, 2013: The contribution of urbanization to recent extreme heat events and a potential mitigation strategy in the Beijing–Tianjin–Hebei metropolitan

area. *Theor. Appl. Climatol.*, **114**, 407–416, <https://doi.org/10.1007/s00704-013-0852-x>.

Wang, P., J. Tang, X. Sun, S. Wang, J. Wu, X. Dong, and J. Fang, 2017: Heat waves in China: Definitions, leading patterns, and connections to large-scale atmospheric circulation and SSTs. *J. Geophys. Res. Atmos.*, **122**, 10 679–10 699, <https://doi.org/10.1002/2017JD027180>.

Wang, W., W. Zhou, X. Wang, S. K. Fong, and K. C. Leong, 2013: Summer high temperature extremes in southeast China associated with the East Asian jet stream and circumglobal teleconnection. *J. Geophys. Res. Atmos.*, **118**, 8306–8319, <https://doi.org/10.1002/jgrd.50633>.

—, —, and D. Chen, 2014: Summer high temperature extremes in southeast China: Bonding with the El Niño–Southern Oscillation and East Asian summer monsoon coupled system. *J. Climate*, **27**, 4122–4138, <https://doi.org/10.1175/JCLI-D-13-00545.1>.

Ward, K., S. Lauf, B. Kleinschmit, and W. Endlicher, 2016: Heat waves and urban heat islands in Europe: A review of relevant drivers. *Sci. Total Environ.*, **569–570**, 527–539, <https://doi.org/10.1016/j.scitotenv.2016.06.119>.

Weisheimer, A., F. J. Doblas-Reyes, T. Jung, and T. N. Palmer, 2011: On the predictability of the extreme summer 2003 over Europe. *Geophys. Res. Lett.*, **38**, L05704, <https://doi.org/10.1029/2010GL046455>.

Wu, G., Y. Liu, B. Dong, X. Liang, A. Duan, Q. Bao, and J. Yu, 2012: Revisiting Asian monsoon formation and change associated with Tibetan Plateau forcing: I. Formation. *Climate Dyn.*, **39**, 1169–1181, <https://doi.org/10.1007/s00382-012-1334-z>.

Xie, Z., and B. Wang, 2018: Summer atmospheric heat sources over the western–Central Tibetan Plateau: An integrated analysis of multiple reanalysis and satellite datasets. *J. Climate*, **32**, 1181–1202, <https://doi.org/10.1175/JCLI-D-18-0176.1>.

Xin, Y., J. Liu, X. Liu, G. Liu, X. Cheng, and Y. Chen, 2022: Reduction of uncertainties in surface heat flux over the Tibetan Plateau from ERA-Interim to ERA5. *Int. J. Climatol.*, **42**, 6277–6292, <https://doi.org/10.1002/joc.7589>.

Xu, X., T. Zhao, C. Lu, Y. Guo, B. Chen, R. Liu, Y. Li, and X. Shi, 2014: An important mechanism sustaining the atmospheric “water tower” over the Tibetan Plateau. *Atmos. Chem. Phys.*, **14**, 11 287–11 295, <https://doi.org/10.5194/acp-14-11287-2014>.

Yanai, M., and G.-X. Wu, 2006: Effects of the Tibetan Plateau. *The Asian Monsoon*, B. Wang, Ed., Springer, 513–549, [https://doi.org/10.1007/3-540-37722-0\\_13](https://doi.org/10.1007/3-540-37722-0_13).

—, S. Esbensen, and J.-H. Chu, 1973: Determination of bulk properties of tropical cloud clusters from large-scale heat and moisture budgets. *J. Atmos. Sci.*, **30**, 611–627, [https://doi.org/10.1175/1520-0469\(1973\)030<0611:DOBPOT>2.0.CO;2](https://doi.org/10.1175/1520-0469(1973)030<0611:DOBPOT>2.0.CO;2).

You, Q., and Coauthors, 2011: Changes in daily climate extremes in China and their connection to the large scale atmospheric circulation during 1961–2003. *Climate Dyn.*, **36**, 2399–2417, <https://doi.org/10.1007/s00382-009-0735-0>.

—, Z. Jiang, L. Kong, Z. Wu, Y. Bao, S. Kang, and N. Pepin, 2017: A comparison of heat wave climatologies and trends in China based on multiple definitions. *Climate Dyn.*, **48**, 3975–3989, <https://doi.org/10.1007/s00382-016-3315-0>.

Zampieri, M., F. D’Andrea, R. Vautard, P. Ciais, N. de Noblet-Ducoudré, and P. Yiou, 2009: Hot European summers and the role of soil moisture in the propagation of Mediterranean drought. *J. Climate*, **22**, 4747–4758, <https://doi.org/10.1175/2009JCLI2568.1>.

Zhang, B., L. Chen, J. He, C. Zhu, and W. Li, 2009: Characteristics of atmospheric heat sources over Asia in summer: Comparison of results calculated using multiple reanalysis datasets. *J. Meteor. Res.*, **23**, 585–597.

Zhang, G., G. Zeng, X. Yang, and V. Iyakaremye, 2022: Two spatial types of North China heatwaves and their possible links to Barents–Kara Sea ice changes. *Int. J. Climatol.*, **42**, 6876–6889, <https://doi.org/10.1002/joc.7617>.

Zhao, C., Y. Yang, Y. Chi, Y. Sun, X. Zhao, H. Letu, and Y. Xia, 2023: Recent progress in cloud physics and associated radiative effects in China from 2016 to 2022. *Atmos. Res.*, **293**, 106899, <https://doi.org/10.1016/j.atmosres.2023.106899>.

Zhong, S., J. He, Z. Guan, and C. Shi, 2008: Interannual variation in rainfall and atmospheric heat sources over the Tibetan Plateau. *Proc. SPIE*, **7085**, 70851C, <https://doi.org/10.1117/12.794008>.

Zhou, T., S. Ma, and L. Zou, 2014: Understanding a hot summer in central eastern China: Summer 2013 in context of multi-model trend analysis. *Bull. Amer. Meteor. Soc.*, **95**, S54–S57, [https://www.researchgate.net/publication/298834543\\_Understanding\\_a\\_hot\\_summer\\_in\\_central\\_eastern\\_China\\_summer\\_2013\\_in\\_context\\_of\\_multimodel\\_trend\\_analysis](https://www.researchgate.net/publication/298834543_Understanding_a_hot_summer_in_central_eastern_China_summer_2013_in_context_of_multimodel_trend_analysis).

Zhou, X., P. Zhao, J. Chen, L. Chen, and W. Li, 2009: Impacts of thermodynamic processes over the Tibetan Plateau on the Northern Hemispheric climate. *Sci. China*, **52D**, 1679–1693, <https://doi.org/10.1007/s11430-009-0194-9>.

Zhu, C., and Coauthors, 2023: Diagnosing potential impacts of Tibetan Plateau spring soil moisture anomalies on summer precipitation and floods in the Yangtze River basin. *J. Geophys. Res. Atmos.*, **128**, e2022JD037671, <https://doi.org/10.1029/2022JD037671>.

Zhu, X., Y. Liu, and G. Wu, 2012: An assessment of summer sensible heat flux on the Tibetan Plateau from eight data sets. *Sci. China Earth Sci.*, **55**, 779–786, <https://doi.org/10.1007/s11430-012-4379-2>.